Ultimately sensitive bioelectronic sensor by materials and device structures design

*Rosaria Anna Picca, Kyriaki Manoli, Eleonora Macchia, Lucia Sarcina, Cinzia Di Franco, Nicola Cioffi, Davide Blasi, Ronald Österbacka, Fabrizio Torricelli, Gaetano Scamarcio and Luisa Torsi,**

Dr. R. A. Picca,[1,2] Dr. K. Manoli,[1] Dr. E. Macchia,[1] L. Sarcina,[1] Dr. D. Blasi,[2] Prof. N. Cioffi,[1,2] Prof. L. Torsi[1,2,5]
[1] Dipartimento di Chimica - Università degli Studi di Bari "Aldo Moro" - Bari (I)
[2] Centre for Colloid and Surface Science - Università degli Studi di Bari "Aldo Moro" Bari (I)
E-mail: luisa.torsi@uniba.it

Dr. Cinzia Di Franco,[3] Prof. Gaetano Scamarcio,[3,4,]
[3] CNR - Istituto di Fotonica e Nanotecnologie, Sede di Bari (I)
[4] Dipartimento di Fisica "M. Merlin" - Università degli Studi di Bari – "Aldo Moro" - Bari (I)

Prof. R. Österbacka[5]
[5] Physics and Center for Functional Materials, Faculty of Science and Engineering – Åbo Akademi University - Turku (FI)

Prof. F. Torricelli[6]
[6] Dipartimento Ingegneria dell'Informazione - Università degli Studi di Brescia - Brescia (I)

Keywords: sensors, organic filed-effect transistors, organic bioelectronics, biosensors, biomarkers

Organic bioelectronic sensors are gaining momentum as they can combine high performance sensing level with flexible large-area processable materials. This opens to potentially highly powerful biomarkers sensing systems for point-of-care health monitoring and diagnostics. Prominent to detect biochemical recognition events are Electrolyte-Gated Organic Field-Effect Transistors (EGOFETs) and Organic ElectroChemical Transistors (OECTs) as they are easily fabricated and operated. Relevantly, the EGOFETs have been shown capable of label-free single-molecule detections even in serum.

This Progress Report aims to provide a critical perspective through an overview of the literature on both EGOFETs and OECTs biosensors. Attention is paid to correctly attribute them to the potentiometric and amperometric biosensor categories which is important to set the right conditions for quantification purposes. Moreover, to deepen the understanding of the sensing mechanisms, with the support of unpublished data, focus is put on two among the most critical

aspects, namely: the capacitance interplay in EGOFETs and the role of faradaic currents in OECTs. The final aim is providing a general rationale encompassing both EGOFETs and OECTs sensors, to improve materials and devices design taking advantage of the processes that enhance the sensing response enabling the extremely high-performance level resulting in ultimate sensitivity, selectivity and fast response.

1. Introduction

Field-effect transistors (FETs) based transduction of biochemical events has being pursued since decades as it can be highly sensitive, selective and fast. Relevantly, both ionic,[1,2] enzymatic[3] as well as immunometric or genomic[4] interactions can be detected. As to sensitivity is concerned, detection limits below pM (10^{-12} mole·l^{-1}) can be achieved with different device structures. The biosensors are endowed with selectivity by integrating a layer of biological recognition elements that are attached to one of the FET electronic interfaces. Last but not least, the real time response of the binding process is generally an extremely fast event even when the recognition involves pM and sub-pM target analyte concentrations.[5–7] This makes bioelectronic approaches very interesting over workhorses in biomarkers detections such as Enzyme Linked Immunoassay (ELISA) known for providing slow responses when assaying concentrations below pM.[8]

Organic based FETs (OFETs) biosensing devices have gathered a lot of attention[9–19] as they typically engage large-area processable semiconductors as channel materials so they can be, in principle, produced at low cost. Moreover, organic semiconductors can be biocompatible and so amenable to be used for implantable bioelectronic systems. In this respect, particularly interesting are the transistors gated *via* an ionically conducting and electronically insulating electrolyte that have been also widely studied as organic bioelectronic devices.[20–30] As sensors, among the others, electrolyte-gated organic field-effect transistors (EGOFETs)[24] have been proposed.[31–33] Relevantly, EGOFET sensors have been proven to reach limit of

detections (LODs) in the 10^{-18} M (aM) range.[34,35] Very recently, they have been proven capable to detect biomarkers at the physical-limit reaching LODs of 10^{-21} M (zM) with a technology called *Single-Molecule with a large Transistor* (SiMoT).[36–39]

Indeed, digitalization is a major driver in biomarkers assay and can enable precision medicine to enter into the everyday clinical practise.[8] Among the single-molecule detection methods proposed so far, only few are, however, exploitable for clinical assays. Large-area organic-bioelectronics is emerging as a cross-disciplinary research field for the development of a platform capable of selective, label-free and fast biomarker detection at the physical-limit in real biofluids. A mass-manufacturable platform with such characteristics holds the potential to bring precision medicine into the everyday medical practice, revolutionizing our current approach to clinical analysis.

In this Progress Report a critical review of the field of organic bioelectronic sensors for biomarkers detection is provided. The aim is to offer elements and insights to better understanding the sensing mechanisms in both the EGOFETs and the Organic ElectroChemical Transistors (OECTs) approaches and eventually to achieve the high-performance detection of biochemical events. Unpublished experiments are also discussed to get an insightful view of still open issues such as the capacitance interplay in EGOFETs and the role of faradaic currents in OECTs detection. The final goal is to provide a more rational view of the device and materials design aspects that can result in extremely high-performance sensing level.

2. The basic features in organic bioelectronic transistors sensors

Organic bioelectronic transistor structures for biosensing assays involve OFETs whose structural peculiar characteristics can vary according to the targeted application. However, they all share at least two features:

- the devices are operated in an electrolyte or even in a body fluid; the strategic design of the materials and of the device structures to achieve stable operation in such conditions are paramount and will be addressed while discussing the different functional regimes;

- the OFETs integrate a layer of biological recognition elements that can selectively bind the analyte of interest. This can be, for instance, a biomarker known to work for diagnosis or prognosis purposes.

In **Figure 1** the essential structures of an OFET comprising a resistor (S and D contacts covered by an organic semiconductor) whose conductivity is controlled by the gate electrode (G) through an electrolyte (*e.g.* water),[22,32,36,40] is shown. For a stable and reproducible operation care must be taken to make sure that the layer of biological recognition elements is covalently anchored to one of the FET electronic interface. Such a layer can be either attached to the gate surface[31,32,41] as shown in **Figure 1a**, or on the FET semiconductor[33,42,43] (**Figure 1b**). In the former case a gold metal surface that can be chemically engineered via thiol-based self-assembled monolayers (SAMs). At variance, the organic semiconductors or other large-area processable materials, such as graphene for instance, can be tailored with different functional moieties to enable the grafting of the bio-recognition elements. While this can be a very versatile approach, it works better with two-dimensional layers as the bio-functionalization can be tailored to involve just the outermost surface of the electronic channel material. In fact, functional groups in the bulk of the organic semiconductor[44] can generate defects in the delocalized electronic system, maybe impacting on the charge carrier mobility.

Many other molecules and biomolecules are present in a biofluid so, as anticipated, to selectively detect an analyte biomarker a recognition-element that binds exclusively the target-biomarker forming a stable complex, is engaged. To this end, selective ion-membranes can be used to sense different ionic spices. For bio-chemical interactions, different kind of bio-recognition elements can be used depending on the nature of the analyte to be detected.

For instance, a specific-capturing antibody is used to bind its antigen-protein biomarker (**Figure 1c**). A peptide with a given sequence of amino-acids works to recognize and sense a complementary peptide biomarker. For genetic (DNA, RNA, aptamer) biomarkers a strand comprising a sequence of nucleotides complementary to those of the biomarker works as the probe recognition-element (**Figure 1d**). An enzyme also acts as recognition-element for its substrate which is the biomarker. As an example, the case of the glucose biomarker and the glucose-oxidase enzyme is shown in **Figure 1e**. In the enzymatic-selective reaction the substrate and the enzyme form an intermediate complex while an electrochemical reaction takes place. In the featured case the substrate is oxidized (gives an electron away) and the enzyme is reduced (receives an electron). Eventually, the substrate turns into the product (glucolactone), that is released by the enzyme. The extra-electron held by the glucose-oxidase enzyme turns, in water, the environmental molecular oxygen into oxygen-peroxide. The enzymatic reaction takes place spontaneously. However, if an electrode, maybe immobilizing the enzyme, is held fixed at the oxygen-peroxide oxidizing potential, a stationary Faradaic-current can be measured which is proportional to the glucose concentration. This is a typical strategy adopted for instance to quantify glucose level in blood.

Organic bioelectronic sensors for ions, antigens, DNA and peptides are generally potentiometric devices, operating along the same principle of the ion-selective electrochemical electrodes. In such biosensor, a zero-current potential (relative to a reference electrode) builds at a selective membrane or at an electrode surface functionalized with biological recognition elements. Upon interaction with the analyte (the species to be detected), is correlated to the analyte concentration by the Nernst equation. In the case of ions interacting with an ion-permeable membrane, the electrochemical potential drop $\Delta\Phi$ across the sensing interface is a quantitative function of the concentrations of a given ion inside [c_0] (reference concentration) and outside [c] a membrane: $\Delta\Phi = \Phi - \Phi_0 = \frac{k_B T}{e} \ln \frac{[c]}{[c_0]}$, with k_B

being the Boltzmann constant, T the temperature, e the elementary charge. In the case of an immunometric or genomic interaction the following holds: the recognition element (R), carries a charge X (R^X) when attached at a given interface in a given solution and interacts with its affinity ligand or probe, the biomarker, (B) that carries a charge Y (B^Y). The resulting complex RB carries a charge W (RB^W) so that $R^X + B^Y \rightleftharpoons RB^W$ with a given equilibrium constant K. In this case the membrane composed of R^X attached to the electronic interface, is the layer of biological recognition elements. The equilibrium of ionic species at this interface is governed by the Donnan equations,[4,41,45] and the quantitative relation between the Φ and the RB^W concentration $[RB^W]$ becomes:

$$\Delta\Phi = \frac{k_B T}{e}\left(\operatorname{asinh}\frac{W[RB]}{2z[c]} - \operatorname{asinh}\frac{X[R]}{2z[c]}\right) \qquad (1a)$$

where z is the valence of the ions in the electrolyte and [c] is the bulk ion concentration. The ΔΦ potential defined in **Equation 1a** can be measured directly or via a FET transducing device as the ΔΦ shift can modulate the source – drain current (I_D) that flows in the electronic channel.

An organic bioelectronic device that involves a redox reaction to selectively detect for instance metabolites such as glucose or lactate, can be operated either as a potentiometric or as an amperometric sensor.[46] In the latter case, a transient current is measured while an external bias is set at a potential larger than the equilibrium value of the redox species, E_0. The correlation between the measured Faraday current (I) and the concentration [c] of the analyte, depends on the measurement set-up. For a chrono-amperometric (I-limit, I_l *vs.* time, t) measurement, the Cottrell equation holds:

$$I_l = (\pi t)^{-1/2} \cdot A \cdot n \cdot F \cdot D^{1/2} \cdot [c] \qquad (1b)$$

where, t is the time, A is the electrode area, n is the moles of exchanged electrodes, F is the Faraday constant and D is the diffusion of the reacting species in the solution. **Equation 1b**, sets that a current flows only if the following conditions are both satisfied:

- the electrochemical reaction takes place at an external bias larger than its electrochemical equilibrium potential or Fermi level, E_0;

- the electrochemical potential is fixed (potentiostatically controlled) during the reaction, regardless of the faradaic current flowing through it.

The first condition is satisfied when the detection is carried out applying an external bias that sets the sensing interface at a potential higher than E_0. For the second condition to hold, a reference electrode such as an Ag/AgCl one, keeps the potential in solution fixed. In a two electrodes cell configuration (one being the reference, *vide infra*), a redox reaction is continuously running within the reference electrode, which sustains a Faradaic current through the working electrode. In a standard three-electrodes electrochemical measurement, this current is limited by a high impedance circuit mesh.[47] In the absence of this element, necessarily, any capacitance at the electrode where the electron transfer occurs, cancels off.[48]

2.1. The essentials in detecting and quantifying analytes and biomarkers

A biomarker is an indicator of the normal physiological or pathogenic state of an organism or of the pharmacologic response to a therapeutic intervention.[49,50] In clinical assays the presence of a biomarker in a biofluid sample is detected, generally with a level of confidence of 99%, by evaluating the LOD[51] that guarantees 1% statistical incidence of false-positive-responses. To this end, negative-control experiments are devised to evaluate the assay level-of-noise. They are performed by assessing the biofluid with a non-recognition element; *i.e. via* a biomolecule that does not form any complex with the targeted biomarker. A zero-response, to be measured in n-plicate ($n \geq 10$), is hence returned. The negative-control statistical functions enable to evaluate the LOD as the zero-response average-value plus three times its standard-deviation. Spurious noise fluctuations (false-positives) are hence limited to 1%. To limit false-negatives also to 1%, the zero-response average plus ten-times its standard-deviation has to be evaluated and defines the limit-of-quantification (LOQ).[51] To quantify a

biomarker an analytical calibration or dose-curve is also invariably needed. This is accomplished by assaying three-five standard-solutions comprising a known amount of the target biomarker. To reproduce other biochemical features of the real-fluid, a phosphate-buffer-saline solution with a pH and a whole ionic concentration (ionic-strength) comparable to those of the sampled biofluid, serves to the scope. Eventually, the biomarker concentration is quantified by comparing its response to those in the dose-curve. Each and every response is to be acquired in triplicates and the associated error defines the assay precision.[14] Samples and standard-solutions aliquots of 100 μl are generally analysed as this is the smallest volume with an associated maximum uncertainty in measuring and transferring is within 1%.

Assays can be performed adopting both label-based or label-free approaches. When a biomarker cannot be directly detected, a label (*i.e.* a fluorogenic-molecule, an isotopic-radioactive-tracer or an electrochemically-active species) is quantitatively associated with it. The biomarker is, hence, quantified by assaying the label instead. At variance, label-free analytical-methods perform the direct measurement of a biomarker intrinsic property, *i.e.* mass, electrical, dielectric, optical *etc*. The need for a labelling-step can be a drawback as it increases the assay complexity adding steps and personnel cost to it.

In clinical practice, to gather enough information to formulate a diagnosis, a number of biomarkers are normally quantified from the same biological sample. This is called multiplexing[52] and requires a technology amenable to be developed into an array of 96 or more transducing-elements, so that the standard solutions, the negative-controls and the sample can be assayed, with all the replicates for each biomarker, at the same time. In **Table 1** the most relevant figures of merit for biosensors are summarized.

Table 1. Figures of merit for performance assessment of biosensor[14,51,53,54]

Figure of merit	Definition
Sensitivity	The slope of the analytical calibration or dose curve. The calibration curve has to encompass at least three orders of magnitudes of concentration dynamic range.

Selectivity	The ability of the biosensor to detect a specific analyte and discriminate it from other species known as interfering. It can be quantified as the ratio between response to the target and to the interference for a given concentration.
Specificity	It is the ultimate limit of selectivity and applies only to a method/sensor, which is capable to detect exclusively the analyte, without suffering for any interference (100% selectivity).
Limit of detection (LOD)	The lowest analyte concentration that can be discriminated from blank (solution with no analyte) at a given confidence level. It can be calculated considering a signal $y_{LOD} = y_c + ks_c$, whereby y_c is the mean signal for control experiment, s_c is its standard deviation, and k is a numerical factor referred to the chosen confidence level (generally, 3).
Limit of quantification (LOQ)	The lowest quantifiable concentration with a given precision and accuracy. It can be calculated as the LOD, using k = 10.
Dynamic range	The concentration range in which the output signal varies in response to different analyte concentrations. It includes the linearity range.
Repeatability	The degree of scattering of the data obtained on successive measurements of a given parameter under the same operating conditions, *e.g.* the response of a single biosensor to the same analyte over time.
Reproducibility	The degree of scattering of the data obtained on measurements of a given parameter under the different operating conditions; *e.g.* the response to the same analyte measured with nominally identical but different biosensors.

2.2. Organic bioelectronic sensors materials and devices operational regimes

Depending on their chemical structures and on the electrolyte in which they work, organic semiconductors can be prevalently ion-permeable or ion-impermeable. It is well known, for example, that when conductive or semi-conductive conjugated polymers undergo an electrochemical oxidation or reduction, meaning they give or receive an electron from an external power supply or from a doping molecule, a stochiometric aliquot of charge compensating anions or cations can drift into the device structure. This occurs, however, if the ions steric hindrance, the chemical affinity and the polymer porosity enable it.[55]

In **Figure 2a** the chemical structure of typical hydrophobic polymers such as poly(3-hexylthiophene-2,5-diyl) (P3HT) or poly [2,5-bis(3-tetradecylthiophen-2-yl) thieno[3,2-b]thiophene] (PBTTT), that are ion-impermeable when operated in aqueous electrolytes, are shown. P3HT and PBTTT form films whose structures are very compact with a rather hydrophobic surface as they are constituted by an elongated π-system, leading to a strong π-π stacking among the polymer chains. Due to their elevate degree of regioregularity and the

presence of aliphatic moieties grafting the semiconductor chain, solution-processed and thermal annealed P3HT and PBTTT films exhibit a well-organized structure with an elevate degree of crystallinity.[56–58] Thus, these polymers, from one hand ensure good hole mobility, on the other hand are not permeable to water and ions.

In **Figure 2b** the structure of the Poly(3,4-ethylenedioxythiophene) polystyrene sulfonate (PEDOT-PSS) also widely used as channel material, is shown. Like many of the elicited conducting polymers, PEDOT-PSS is ion-permeable in e water solution because of its porous and hydrophilic structure enables ions to enter into the bulk of the film. This makes it a typical example of an organic mixed ionic/electronic conductor. It is composed by an overall amorphous blend of a conjugated polymer (PEDOT) and a negatively charged polyelectrolyte (PSS) acting as a dopant for the PEDOT. The PEDOT-PSS films show high p-type conductivity when small domains of π–π stacked PEDOT nanofibrils[59,60] (blue strips in the bottom of Figure 2b) surrounded by the PSS polymer form. This occurs when PEDOT-PSS is spin-coated from a water solution added with dimethylsulfoxide (DMSO), as in this case the solvent evaporation is slowed down enabling PEDOT to self-assemble into small crystalline domains.[27,28]

Based on the ionic permeability of the electronic channel materials, OFETs working in an electrolyte can be classified into two categories.[24] In **Figure 2c**, an EGOFET comprising an ion-impermeable channel material is shown. In this case two-dimensional (2D) capacitances, labelled C_G (gate capacitance) and C_{OSC} (organic semiconductor capacitance) are shown. A bio-layer attached to the gate is shown here along with its capacitance C_{BIO} in series with the previous ones; similarly, a structure where the channel material is biofunctionalized can be used. EGOFETs based on electronic-channel materials such as P3HT[36–39] and graphene,[34] have been proposed and EGOFETs are operated almost invariably as potentiometric sensors.

When the channel material is ion-permeable, the bioelectronic device is commonly addressed as Organic ElectroChemical-Transistor (OECT).[61] PEDOT-PSS or conducting polymers such as polypyrrole[61] or polythiophene are generally used as channel materials. In the OECT structure, C_{OSC} extends into the bulk of the channel resulting in a three-dimensional (3D) capacitance of tens of $F \cdot cm^{-3}$.[62,63] Typically, OECTs are engaged in the sensing of electroactive species such as ions or metabolites. In the latter case, the interaction with an enzyme grants a selective response, while for ions detection selective membranes are engaged. OECTs can be operated as potentiometric and amperometric sensors. When operated as potentiometric sensors, their basic functional mechanism can be featured as in Figure 2c. In this case, no conceptual difference exists with EGOFETs, the only difference being C_{OSC} switching from a 2D to a 3D capacitance. Indeed PEDOT-PSS has been shown capable to work in an EGOFET bioelectronic sensing structure.[35]

Conceptually different is the case of OECTs operated as amperometric sensors. A possible sensing mechanism for this type of biosensor is schematically featured in **Figure 2d** where an oxidation reaction takes place in solution with an electron being transferred to the PEDOT-PSS film. This could be the case, for instance, when the oxygen-peroxide oxidizing reaction is used in the selective detection of a metabolite involving an oxidase enzyme such as the elicited glucose-oxidase to assay glucose (Figure 1e), the choline oxidase to assay the acetylcholine neurotransmitter or the urate oxidase to assay uric acid. Invariably, the enzyme can be attached to the organic semiconductor surface or to the gate surface.

It is worth to mention that the categorization of EGOFETs working with ion-permeable materials and OECTs with ion-permeable ones is not related to the channel material itself but rather to the system comprising the channel material and the ionic species in the electrolyte.

Indeed, while PBTTT is ion-impermeable to hydroxides it becomes permeable to picric acid anions. Hence a 2D or a 3D capacitance can be installed in the same device by just changing

the ions of the electrolyte.[64] Moreover, a capacitance can switch from a 2D to a 3D by just tuning the side chains of a polymer channel material.[65]

3. Electrolyte-gated organic field-effect transistor sensors

The first devices that will be reviewed are the EGOFETs that, as anticipated, have been successfully engaged as label-free bioelectronic sensors exhibiting limit-of-detections down to the zM - aM level also in real bio-fluids. This makes them not only the highest performing bioelectronics sensors, but a promising single-molecule detecting technologies.

In an EGOFET device (or in an OECT operated in the potentiometric mode), upon gate biasing, transient ionic currents allow the electrolyte ions to accumulate at the gate/electrolyte and electrolyte/semiconductor interfaces, eventually forming the already introduced C_G, C_{BIO} and C_{OSC} 2D capacitances (Figure 2c). As they are both of the order of tens of $\mu F/cm^2$, an EGOFET can operate in the sub-volt regime.[6] The field-induced carriers, drifting between the source and drain contacts under the V_D bias originate the EGOFET I_D output current. Importantly, the biological species involved in EGOFETs should be antibodies (Figure 1c) or genomic-probes (Figure 1d) so as the interaction with the biomarkers does not produce any Faradaic-current that would generate a high gate leakage current (I_G). Such a current will affect the 2D capacitances compromising the capacitance coupling that, as it will be discussed later, are the basis for the FET-induced enhancement in these bioelectronic sensors. The case of OECTs detecting electrochemical reactions, obviously generating a Faradaic current, and operated in the potentiometric mode will be addressed in Section 5.

In **Figure 3** two examples of EGOFETs, involving either a biofunctionalization of the gate or the organic semiconductor, operated in potentiometric mode are presented. In **Figure 3a** an EGOFET bioelectronic sensor to detect the dopamine neurotransmitter down to pM concentration by means of a thiol based SAM on a gold gate electrode[31] is shown. In the

seminal work by the Biscarini's group, the SAM attached to the gate (**Figure 3b**) comprises boronic acids functionalities that exhibits a high chemical affinity towards molecules like dopamine. In this sense the boronic acid functional moiety can act as a recognition element for dopamine. Upon binding, a negatively charged boronic ester is formed whose charge is screened by the amine group of the dopamine and an interfacial dipole eventually forms. In **Figure 3c** the potential changes occurring upon dopamine binding are shown. Due to the 2D capacitances that are formed upon the application of the V_G bias (Figure 2c), voltage drops at the gate–liquid interface and at the liquid–semiconductor interface occurs. The potential drop at the liquid–semiconductor interface governs the surface charge density of carriers in the channel and defines the intensity of the I_D current that flows upon V_D bias application. When the dopamine sensing induced dipole forms, the potential drop at the gate–liquid interface increases and thus a higher voltage has to be applied to induce at the same amount of carrier density in the channel. Even when concentrations as low as few pM of dopamine are sensed sizable changes in EGOFET transfer characteristics, I_D vs. V_G at fixed V_D (**Figure 3d)** were measured.

In **Figure 3e** an EGOFET structure for the detection of procalcitonin which is a marker for sepsis is shown.[42] In this example the layer of biological recognition element (the procalcitonin specific antibody) is attached, through direct physical adsorption, to the surface of the spin-coated P3HT organic semiconductor. This is followed by the deposition of the bovine serum albumin serving as the blocking agent to prevent non-specific adsorption of bio-spices that are not the biomarker. The entire immunosensor fabrication process require less than an hour to be completed before the analyte sensing. The sensing transfer characteristics measured at different procalcitonin concentration are given in **Figure 3f**. The EGOFET immunosensor showed excellent performance level including a LOD as low as 2.2 pM, which is also within the range of clinical relevance for procalcitonin detection. Control experiments also proved that the immunosensor was highly selective.

In both these cases the devices are operated as potentiometric sensors. It is to point out that the dependence of I_D versus the logarithm of the analyte concentration can be straightforwardly modelled with Equation 1a only when the direct sensing of an analyte is performed. This is the case for EGOFETs or OECTs detecting ions.[2,46] When the detection of an analyte is performed via a biochemical binding reaction, the binding affinity equilibrium reaction has to be considered too.

This session ends by recalling two of the few bioelectronic sensors operated as EGOFETs or in the potentiometric mode, that engage a PEDOT-PSS electronic material. A functionalized gold electrode was engaged to perform DNA detection. The sensing mechanism involves the modulation of the surface potential of the gate electrode induced by the immobilization and the hybridization of DNA molecules on the gate surface. The device was able to detect DNA targets at concentrations as low as 1 nM and its detection limit reached 10 pM by pulse-enhanced hybridization of DNA.[66] Even better performance level was achieved with an EGOFET operating with a PEDOT-PSS channel material for the detection of immunoglobulin G (IgG) with an unprecedented aM detection limit.[35] In this case the anti-IgG is the recognition element that is attached to the gold gate and the PEDOT-PSS is capacitively coupled to the sensing gate. It is important to remark that in all the EGOFETs discussed no electrochemical reaction took place as all the bio-recognition events involved conformational changes of an antibody or of a DNA probe where no electron transfer occurs. The cases when a potentiometric sensing is performed with PEDOT-PSS FETs involving electrochemical reactions will be addressed in section 5.

In **Table 2** the most relevant EGOFET bioelectronic sensors published so far are listed including the relevant figures of merit.

Table 2. Selected examples of EGOFETs along with figures of merit

Analyte / biomarker	Sensing element with bio-recognition species	Gate / Channel material	Electrolyte	Dynamic range	LOD	LOQ	REF
Carvone	Au_ (SAM of 3MPA/F88WH(6) pOBP	Au_SAM/ PBTTT-C14	H_2O	1 pM -5nM	50 pM	150 pM	[32]
Procalcitonin (PCT)	P3HT/anti–PCT (CALCA 4A6)	Au/P3HT-anti PCT	PBS (pH= 7.4)	0.8 pM - 5 nM	2.2 pM	N.A.	[42]
Dopamine	Au_ (SAM of CA/BA)	Au_SAM / P3HT	PBS (pH= 8.5)	1 pM -1mM	1 pM[a)]	N.A.	[31]
Thyroid stimulating hormone (TSH)	Graphene_(SAM of thiol–PEG- F(ab′)2 -anti-TSH)	Ag/AgCl/Graphene-SAM	PBS (pH= 8)	0.1 fM- 10 nM	0.8 fM in serum	N.A.	[67]
Odorant amyl butyrate (AB)	Graphene- 2AG1 (hOR2AG1: OR)	Graphene		0.04 fM- 4 nM	0.04 fM	N.A.	[34]
Anthrax toxin-protective antigen (PA)	Graphene_ SS-DNA-protective antigen (PA63 5-12) aptamer & Graphene-sandwich structure of aptamer/PA/aptamer-AuNPs,	Pt/ Graphene_ SS-DNA-protective antigen (PA63 5-12) aptamer	10 μM PBS (pH= 7.4)	12 aM – 120 fM	12 aM & 1.2 aM	N.A.	[6]
anti-human Immunoglobulin G (IgG)	Au_ (SAM of 3MPA_11MUA/anti-h-IgG)	Au_SAM/ PEDOT:PSS	PBS (pH= 7.4)	6 aM -60 pM	6 aM	N.A.	[35]
D-phenylalanine (D-Phe) and L-phenylalanine (L-Phe) enantiomers	Im^+-Ph-β-CD	Si/SiO_2 bottom gate / $F_{16}CuPc$	H_2O	0.01 aM – 1 nM	aM	N.A.	[68]
C-reactive protein (CRP)	Au_ (SAM of 3MPA_11MUA/anti-CRP)	Au_SAM / P3HT	H_2O	0.6 aM -0.1 fM	590 zM in saliva	N.A.	[39]
anti-human Immunoglobulin G (IgG)	Au_ (SAM of 3MPA_11MUA/anti-h-IgG)	Au_SAM / P3HT	H_2O	10 zM -1 fM	10 zM ; 250 zM in serum	N.A.	[36]

[a)] Lowest detected concentration

3.1 Label-free detection of biomarkers at the single molecule level

A relevant question is why it is worth to detect biomarkers at the single-molecule level in a real bio-fluid of a volume of 100 μl. It is received that digital tracking of a biomarker from its physiologic to its pathogenic level will enable to define, with the ultimate sensitivity and resolution, the healthy to diseased onset in an organism. Early diagnostic in progressive diseases would, hence, become possible well before any symptom appears. Single-molecule biomarker detection would also enable a greater level of control over the effects of a

pharmacological therapy as well as over the recrudescence of tumours after surgical resection. It would further enable biomarkers quantification non-invasively in readily available biofluids such as saliva, sweat or even tears where they can be present at much lower concentrations. Along the same line, it would make ultrasensitive liquid biopsy, *i.e.* the assay of peripheral biofluids such as plasma, serum or even saliva, a feasible medical procedure replacing the invasive and much more dangerous direct inspection of diseased tissues.

In general, for a single-biomolecular reaction to occur, the two reagents need to be confined in an adequately small volume for a sufficiently long time. The recognition-element can be attached on a surface that serves as detecting interface. Regardless, the interaction cross-section of the two reagents is to be reasonably high. In this respect, a volume of 1 μm^3 (1 femtoliter - fl) has been proven sufficiently small for a single enzyme to interact with its substrate (present in excess concentration though) on the minute time-scale.[69,70] Indeed, a solution comprising $n = 1 \pm 1$ ($\sqrt{n}$ = Poisson error) molecules in each 1fl sub-volumes has a concentration of $\sim 1 \cdot 10^{-9}$ mol $\cdot$ l^{-1} (nM). Smaller volumes (attoliter, *al*, or zeptoliter, *zl*) each occupied by a single molecule, entails even larger concentrations. Since the number of molecules in a volume V = 100 μl of a solution of molar concentration [c] is $n=[c]\cdot V\cdot N_A$ (N_A=Avogadro's number), 1 nM equals $\sim 10^{11}$ molecules or, equivalently, $\sim 10^{11}$ 1 fl sub-volumes altogether make 100 μl. As two molecules need to be confined in a volume of 1 fl or smaller to rapidly interact, at least one of them is to be present at a concentration of 1 nM. Every 1 fl (or lower) statistically contains one reagent, so wherever the other single reagent is, there is always one fl sub-volume comprising both reagents. A single-molecule interaction can, therefore, occur when the recognition-elements are present at nM concentration (or higher) along with a single biomarker or the opposite way around. In clinical assays the former is to be preferred. However, if a 100 μl sample contains one single biomarker, a platform with a limit-of-detection of 10 zM is necessary, which is challenging. On the other

hand, approaches entailing few recognition-elements need biomarkers at nM concentration or higher. They are, hence, inherently unfit to sense a single-molecule in a bulk milieu. Moreover, a number of high-throughput analytical-clinical methods can detect biomarkers at the nM level or lower. Among the others, there is the ELISA platform introduced below.[71,72] Indeed, label-free investigations reaching single-molecule resolution have been performed, so far, by means of nanometric probes. A paradigmatic example is the carbon-nanotube FET detection of a single DNA biomarker. The nanotube bears, covalently attached to a point-defect, few single-stranded DNA probes complementary to the biomarker. Through the source and the drain contacts the current flowing in the nanotube, gated through an electrolyte is measured.[73] When one of the biomarkers in the 1 μM solution is in contact with the nanotube, it hybridizes the probe forming a complex and, as a result, the conductance of the nanotube changes. Given the comparable size between the molecule to be detected and the transducing interface, the signal-to-noise is acceptable to detect the event. However, on a nanometric device, the number of recognition-elements is limited by the size of the transducing nanointerfaces. The lateral resolution is about 10-100 nm delimiting a 1 zeptoliter - attoliter volume. Necessarily, the concentration of biomarkers ranging in the pM-mM regime (10^8 - 10^{17} molecules in 100 μl) is needed for a binding event to occur. This approach can be of relevance to study the peculiarities of rarer events that would be lost in ensemble measurements where the information derived is representative of the average most common events. As an instance, in the case of the nanotube transistor,[72] two-level conductance fluctuations, associated with one-single biomarker binding and unbinding, are recorded in the ms time-framework when 3 ml of 1 μM DNA biomarker solution is used. This corresponds to ~ $2 \cdot 10^{15}$ DNA biomolecules occupying the 10^{14} $(100\ nm)^3$ volumes (attoliters), available in 100 μl. Thus, ~ 20 DNA biomarkers statistically resides in close-proximity of the detecting interface generating a train of single-molecule binding-unbinding events that can be

individually recorded and studied, wherever the nanometric transistor is located. The response generated at each single-interaction enables the measurement of key interaction parameters, such as the rate constants and activation energies that can be correlated to those of the whole ensemble of events evidencing the peculiar behavior of rarer events.

While the importance of such studies capable to spot rarer features to address fundamental investigation of biomolecular interactions is beyond doubt, it is a fact that far- and near-field approaches cannot address detections at the 10 zM limit-of-detections. This is because there would be one probability over 10^{11} to place the microscope objective or one over 10^{14} chances to accommodate the detecting nano-interface in the inspected 100 μl bulk, exactly in the 1 fl or 1 al sub-volume where the biomarker is placed. Hence, they are not suitable to be engaged in clinical-assays.

3.2 Ultra-sensitive bio-detections with millimetre wide OFETs

Table 2 shows that EGOFETs can detect down to the sub aM regimes. As in 100 μl of a 10 aM solution there are around 10^3 particles, it means being able to detect at the physical limit. An example of such ultra-sensitive devices is the SiMoT EGOFET,[37] where the gate is bio-functionalized[36,38,74] with $2 \cdot 10^{12}$ recognition-elements covalently attached to a 0.5 cm^2 gold-gate, which is equivalent to ~10 nM recognition-elements that would be available for the binding in 100 μl. The binding is very fast as it occurs even at very low concentration in the minute time-scale. This confirms the already highlighted trend, peculiar of many other FET transducing interface.[5–7]

In **Figure 4a** the basic structure of the *SiMoT* EGOFET device is provided while in **Figure 4b** the real device is featured. **Figure 4c** shows the Human-Immunoglobulin-G (H-IgG) protein assay in the 0 -100 zM concentration range. The anti-Human-Immunoglobulin-G specific-capturing-antibodies served as recognition-elements. The responses measured at 10 zM and

20 zM (1±1 particles) are at the limit-of-detection and prove that a large millimeter sized EGOFET can detect a single protein. The EGOFETs can perform label-free detections at the physical-limit also in a real biofluid (**Figure 4d**). A bovine blood-serum added with different aliquots of human-IgG (H-IgG) biomarker is assayed (red-squares) while Human-Immunoglobulin-M served as non-recognition elements in the control-experiment (back-circles). A limit-of-detection of 250 zM, corresponding to 15 ± 4 proteins, is evaluated. More in detail, the gates are exposed either to standard solutions of the biomarker in phosphate-buffered saline (PBS) or in the real biofluid, while the actual change in its electrochemical potential is measured in water to minimize the Debye screening length. The SiMoT EG-FET could detect at the physical limit also Immunoglobulin-M,[38] C-reactive protein in saliva,[39] and HIV1 P-24[75] while unpublished data are available on the detection of MUC1, streptavidin and avidin proteins as well as on peptides designed to mimic protein post-translational modifications and KRAS DNA.

Other selected examples of extremely sensitive EGOFETs are provided in **Figure 5**. In **Figure 5a** a graphene EGOFET bioelectronic odors sensor is shown. The 2AG1-human-olfactory-receptors (hOR2AG1), serving as recognition-elements, are attached to the outermost layer of a graphene double-layer channel-material (**Figure 5b**). These receptors selectively bind the amyl-butyrate odorant. Both an oxygen-plasma-treated graphene bi-layer surface, resulting in a p-type layer, and an ammonia-plasma-treated graphene, resulting in a n-type one, are used to chemically bind the recognition elements. As many as ~ $5 \cdot 10^9$ olfactory-receptors are attached (density of $5 \cdot 10^{11}$ cm^{-2}), resulting in an equivalent concentration of recognition elements of ~50 pM in 100 μl. A PBS solution at pH=7.4, serves as gating electrolyte. In **Figure 5c** the responses of the bioelectronic-nose, evaluated as the I_D source-drain current relative variations upon exposure to different concentrations (40 aM - 400 pM) of the amyl-butylate odorant, are shown. The red-trace is measured on the p-type graphene

while the blue-trace is relevant to n-type one; as expected, the two responses are opposite in sign. The black-trace is the response of a pristine graphene, not binding any recognition element, hence it is taken as the noise level. The evaluated limit-of-detection is as low as 40 aM and a rapid response-time of less than 1s is recorded. The label-free sensing-mechanism, involving only one step, is ascribed to a structural rearrangement of the olfactory-receptor that becomes negatively charged upon selectively binding the biomarker. This electrostatic change induces an accumulation of positive-charge-carriers in the graphene-channel resulting in an increase of the source-drain current I_D in the p-type graphene-channel, while a decrease is measured with the n-type surface.[34]

Capacity coupled configuration that comprises a chiral bio-recognition layer also performed at extremely low detection limit.[68] In **Figure 5d** the device structure is provided showing a bottom gate top contacts configuration. A β-cyclodextrin (β-CD) derivative, namely a mono-6-deoxy-6-(1-allylimidazolium)-per(3,5-dimethyl)-phenylcarbamoylated-β-CD (Im^+-Ph-β-CD) is deposited directly on the copper hexadeca-fluoro-phthalocyanine ($F_{16}CuPc$) organic semiconducting layer. While this is not an EGOFET device (it is gated *via* SiO_2), it is operated in water and a capacity coupling exists among the gate, the electronic channel and the chiral biological recognition elements laying on top. In this respect, the sensing mechanism can be assimilated to that of an EGOFET. In **Figure 5e** the FET drain current as a function of time changes upon exposure of the bioelectronic device to the D-phenylalanine (D-Phe) and L-phenylalanine (L-Phe) enantiomers is shown. Not only chiral differential detection is demonstrated but also detection limits down to 0.01 aM.

So, the millimeter size electrolyte-gated OFETs shown in Figure 4 and Figure 5 are:

- label-free and involve binding reactions that are not electrochemical in nature;

- engage an extremely large number of biological recognition elements.

Notably, they can detect biomolecules reaching physical limit even in a real-biofluid. These are major advancements that call for a better understanding of the EGOFET sensing mechanisms.

4. The enhanced EGOFET sensor response

The amplification steps that enable EGOFET bioelectronic-sensors to detect 1-10^3 binding-events with a wide-surface comprising billions to trillions recognition-elements are here addressed. While studies are still on-going, plausible mechanisms involve a capacity-coupled FET-transduction and a hydrogen-bonding network enabled cooperative-effects. To properly address them, deepening into EGOFETs material-science and devices-operational aspects is required.

4.1 The interplay between the series of gating capacitances

Biosensors based on EGOFETs translate biochemical events taking place at the gate/electrolyte and/or at the electrolyte/organic-semiconductor (EL/OSC) interfaces in an electronic drain-source current I_D. As anticipated the transduction is due to the capacity coupling between the bio-layer and the channel material and a simplified equivalent circuit of an EGOFET is given in **Figure 6a** for the case of the biolayer attached to the gate.

The EGOFET is modeled as a field-effect transistor with a capacitance C_{OSC}, a resistor R_{EL} accounting for the ion movement through the electrolyte and a gate capacitance C_G. When the bio-layer is considered C_{BIO} is included. For the sake of simplicity in the following C_G and C_{OSC} include the contribution form the bio-layer attached to either one interfaces. So, when the biolayer is anchored to the gate $C = C_G + \Delta C_{BIO}$, $\Delta\Phi = \Delta\Phi_0 + \Delta V_{BIO}$ and when it is at the OSC, $C = C_{OSC} + \Delta C_{BIO}$, $V_T = V_{T0} + \Delta V_{BIO}$ (C being the total capacitance and V_{T0} the

threshold voltage before the binding). Indeed $\Delta\Phi$ given by Equation 1a, accounts for the dependence on the analyte concentration.

At the steady-state conditions (*viz.* in the typical operating potentiometric conditions of EGOFET biosensors) the electrolyte resistor R_{EL} can be neglected while the electric-double-layer capacitances C_{OSC} and C_G are the design variables to enhance the EGOFET biosensor response. We note that in EGOFETs R_{EL} can be neglected by waiting enough time for the transient ionic current to extinguish once the charge-double-layers are formed. For a potentiometric OECT, it is critical to make sure that no transient or, even worst, stationary faradaic I_G current flows. Assuming, for the sake of simplicity, a constant electronic charge carrier mobility μ into the organic semiconductor, the drain current can be described by solving the drift-diffusion, Poisson and continuity equations[45] and reads:

$$I_D = \frac{W}{L}\mu \frac{C_{OSC}}{A_{OSC}} (V_{EL} - V_T)V_D \qquad \text{if } V_{EL} - V_T \geq V_D \qquad (2a)$$

$$I_D = \frac{W}{2L}\mu \frac{C_{OSC}}{A_{OSC}}(V_{EL} - V_T)^2 \qquad \text{if } V_{EL} - V_T < V_D \qquad (2b)$$

where W is the channel width, L is the channel length, A_{OSC} is the OSC area, V_{EL} is the potential in the bulk of the electrolyte, V_T is the threshold voltage, V_D is the drain voltage, and we assume that the source electrode is connected to the ground, *viz.* $V_S = 0$ V. It is worth noting that V_T depends on the electrolyte and semiconductor material parameters such as the bulk ion concentration, the trapped charge into the OSC and the surface charge at the EL/OSC interface. V_{EL} can be related to the external applied voltage by considering the capacitive couplings and reads:

$$V_{EL} = \frac{C_G}{C_G + C_{OSC}}(V_G + \Delta\Phi) + \frac{C_{OSC}}{C_G + C_{OSC}} V_{OSC} \qquad (3)$$

where V_G is the gate voltage, $\Delta\Phi$ for the amount of surface charge and charge distribution on the gate electrode and depends on the biological recognition event (and hence on the analyte concentration) and V_{OSC} is the potential along the channel. V_{OSC} depends on the EGOFET

operating conditions: $V_{OSC} \cong (V_D + V_S)/2$ in linear region of operation where the channel is fully accumulated from the source to the drain, and $V_{OSC} \cong (2/3)\ V_S$ in saturation region where the charge accumulation along the channel extends of about 2/3 of the channel length until reaching the depletion at the drain side. By remembering that $V_S = 0$ and $V_D << V_G$ when the EG-FET is operated in linear region results that $V_{OSC} \cong 0V$ and **Equation 3** simplifies as follows:

$$V_{EL} \cong \frac{C_G}{C_G + C_{OSC}}(V_G + \Delta\Phi) \qquad (4)$$

By inserting **Equation 4** into **Equation 2a** and **Equation 2b**, we obtain an expression of the drain current as a function of the key interface parameters affected by the biorecognition events:

$$I_D = \frac{W}{L}\frac{\mu}{A_{OSC}}\frac{C_G C_{OSC}}{C_G + C_{OSC}}\left[V_G + \Delta\Phi - \left(1 + \frac{C_{OSC}}{C_G}\right) V_T\right] V_D \qquad \text{if } V_{EL} - V_T \geq V_D \qquad (5a)$$

$$I_D = \frac{W}{2L}\frac{\mu}{A_{OSC}}\frac{C_G^2 C_{OSC}}{(C_G + C_{OSC})^2}\left[V_G + \Delta\Phi - \left(1 + \frac{C_{OSC}}{C_G}\right) V_T\right]^2 \qquad \text{if } V_{EL} - V_T < V_D \qquad (5b)$$

Since in EGOFET biosensors either the gate and/or the semiconductor can be biofunctionalized, the overall biosensor performance can be enhanced by means of a suitable design of C_G and C_{OSC} with ΔC_{BIO} contribution included in either one. To gain more insight on the interplay between C_G and C_{OSC}, we performed 2D numerical simulations by solving the Nernst-Planck-Poisson equations into the electrolyte domain coupled with the drift-diffusion Poisson equations into the semiconductor domain. It is worth noting that all the simulations are performed in the case of a hole-transporting semiconductor with $V_D = -0.1V$ and the bulk ion concentration is equal to 10^{-7} M, typical of pure water.

Figure 6b shows the calculated electric potential along the electrolyte domain in the case I) $C_G >> C_{OSC}$, II) $C_G \sim C_{OSC}$, and III) $C_G << C_{OSC}$. The corresponding ion and the hole charge distributions are displayed in **Figures 6c**, **Figures 6d** and **Figures 6e**.

When $C_G >> C_{OSC}$ (case I, Figure 6c) the potential drop at the gate/EL interface is negligible (few millivolts), about 25% of the applied V_G drops on the EL/OSC interface and 75% of V_G drops on the OSC. Figure 6c shows that the hole charge density accumulated into the OSC at the EL/OSC interface is as high as 10^{20} cm^{-3}, which results in a large drain current. When $C_G \sim C_{OSC}$ (case II, Figure 6d) about 50% of V_G drops on the EL, about 0.15 V at the gate/EL interface and 0.15 V at the EL/OSC interface and electrical-double layers at the corresponding interfaces are formed. The remaining 50% of V_G drops on the OSC, and this results in a hole charge density of about 10^{19} cm^{-3} (Figure 6d). With respect to the case I, the hole concentration is lower and therefore, for a given V_G, a lower drain current is obtained.

When $C_G << C_{OSC}$ (case III, Figure 6e) about 60% of the applied V_G drops at the gate/EL interface, 10% of V_G drops at the EL/OSC interface and the remaining 30% drops within the OSC. Figure 6e shows that there is a very weak hole accumulation in the OSC at the EL/OSC interface and the maximum hole density is lower than 10^{15} cm^{-3}. The EGOFET is operated below threshold (subthreshold region) and the drain current is very limited. Under this condition I_D measured in EGOFETs is typically comparable with the leakage gate current. Therefore, case III is not of practical interest because reliable biosensing cannot be performed. Focusing on the cases I and II, it is very interesting to relate these conditions with the simplified Equation 6 and Equation 7 to obtain key guidelines to design high-performance EGOFETs biosensors.

In case I $C_G >> C_{OSC}$ hence $C_G + C_{OSC} \cong C_G$, Equation 5a and Equation 5b becomes:

$$I_D = \frac{W}{L} \mu \frac{C_{OSC}}{A_{OSC}} [V_G + \Delta\Phi]V_D \qquad \text{if } V_G - V_T \geq V_D \qquad (6a)$$

$$I_D = \frac{W}{2} \mu \frac{C_{OSC}}{A_{OSC}} [V_G + \Delta\Phi]^2 \qquad \text{if } V_G - V_T < V_D \qquad (6b)$$

Interestingly, **Equation 6a** and **Equation 6b** show that I_D is independent of C_G. This has important implications for the EGOFET bioelectronic sensor design considering that, in principle, the biorecognition layer can be integrated on the gate or on the OSC surface.

In the case the biolayer is on the gate electrode (as depicted in Figure 2c), the variation of the surface charge and/or charge distribution, associated with ΔC_{BIO}, results in a variation of the gate electrode work function (*viz.* $\Delta\Phi = \Delta\Phi_0 + \Delta V_{BIO}$) which is eventually displayed in a variation of the drain current as displayed in **Equation 7a** and **Equation 7b**:

$$I_D = \frac{W}{L}\,\mu\,\frac{C_{OSC}}{A_{OSC}}[V_G + \Delta\Phi_0 + \Delta V_{BIO}]V_D \qquad \text{if } V_G - V_T \geq V_D \qquad (7a)$$

$$I_D = \frac{W}{2}\,\mu\,\frac{C_{OSC}}{A_{OSC}}[V_G + \Delta\Phi_0 + \Delta V_{BIO}]^2 \qquad \text{if } V_G - V_T < V_D \qquad (7b)$$

while a variation of the gate capacitance due to the biorecognition events cannot be detected (*viz.* $\Delta I_D / \Delta C_{BIO} = 0$).

At variance, when the biolayer is on the OSC a variation of the biolayer capacitance (ΔC_{BIO}) results in a variation of the EL/OSC capacitance, which is displayed in I_D:

$$I_D = \frac{W}{L}\,\mu\,\frac{(C_{OSC}-\Delta C_{BIO})}{A_{OSC}}[V_G + \Delta\Phi_0]V_D \qquad \text{if } V_G - V_T \geq V_D \qquad (8a)$$

$$I_D = \frac{W}{2L}\,\mu\,\frac{(C_{OSC}-\Delta C_{BIO})}{A_{OSC}}[V_G + \Delta\Phi_0]^2 \qquad \text{if } V_G - V_T \geq V_D \qquad (8b)$$

We can conclude that in the case of EGOFET biosensors with $C_G >> C_{OSC}$ it is possible to probe with high sensitivity biochemical events resulting in:

- variations of the surface charge and/or charge distribution (ΔV_{BIO}) when the biolayer is on the gate electrode (Equation 7a and Equation 7b);
- variation of the biolayer capacitance (ΔC_{BIO}) when the biolayer is on the OSC (Equation 8a and Equation 8b).

In case II $C_G \sim C_{OSC}$, the biolayer can be anchored to the gate ($C_G = C - \Delta C_{BIO}$, $\Delta\Phi = \Delta\Phi_0 + \Delta V_{BIO}$) or to the OSC ($C_{OSC} = C - \Delta C_{BIO}$, $V_T = V_{T0} + \Delta V_{BIO}$ with C being the total gating

capacitance before the binding). Assuming that the biorecognition events result in a small variation of the capacitance, namely $\Delta C_{BIO} / C << 1$, after straightforward rearrangement of Equation 5a and Equation 5b the EGOFET drain current in linear and saturation regions results:

$$I_D \cong \frac{W}{L} \mu \left(\frac{C-\Delta CBIO}{2\, A_{OSC}}\right) \left[V_G + \Delta\Phi_0 + \Delta\Phi_{BIO} - \frac{3}{2}V_{T0}\right] V_D \qquad \text{if } V_G - V_T \geq V_D \qquad (9a)$$

$$I_D \cong \frac{W}{2L} \mu \left(\frac{C-\Delta C_{BIO}}{4\, A_{OSC}}\right) \left[V_G + \Delta\Phi_0 + \Delta\Phi_{BIO} - \frac{3}{2}V_{T0}\right]^2 \qquad \text{if } V_G - V_T < V_D \qquad (9b)$$

when the biolayer is anchored to the gate and

$$I_D \cong \frac{W}{L} \mu \left(\frac{C-\Delta CBIO}{2\, A_{OSC}}\right) \left[V_G + \Delta\Phi_0 - \frac{3}{2}(V_{T0} + \Delta V_{BIO})\right] V_D \qquad \text{if } V_G - V_T \geq V_D \qquad (10a)$$

$$I_D \cong \frac{W}{2L} \mu \left(\frac{C-\Delta C_{BIO}}{4\, A_{OSC}}\right) \left[V_G + \Delta\Phi_0 - \frac{3}{2}(V_{T0} + \Delta V_{BIO})\right]^2 \qquad \text{if } V_G - V_T < V_D \qquad (10b)$$

when the biolayer is anchored to the OSC.

By comparing **Equation 9a** with **Equation 10a** and **Equation 9b** with **Equation 10b** it can be noted that in case II ($C_G \sim C_{OSC}$) the biofunctionalized gate EGOFETs show the same sensitivity of a biofunctionalized OSC EGOFETs and the variation of the biolayer capacitance results in a variation of the EGOFET transconductance ($g_m = dI_D/dV_G$), *viz.* of the slope of the I_D-V_G transfer characteristic. On the other hand, when the biochemical events result in a variation of the surface amount of charge and/or charge spatial distribution, a biofunctionalized OSC provide a larger sensitivity.

It is worth noting that, from the sensing point of view, the I_D output current, being modulated also by the above described interplay between C_G, C_{OSC} and C_{BIO} can be sensitive to the dielectric changes occurring in the layer of bio-recognition elements upon binding of a marker. This feature is peculiar of EGOFETs and does not hold, for instance, in MOSFET based sensors.[2] Here, in fact, the gating capacitance is buffered by the very low-k oxide layer whose capacitance is unaffected by the changes occurring in the biological layer or in the ion-

selective membrane when they bind markers or uptake ions. So, while an EGOFET can return information on both the dielectric and electrostatic changes occurring in the biolayer upon binding of the marker, MOSFET sensors are limited to transducing, as a V_T shift, only electrostatic ones. This feature makes MOSFET sensors not best suited to detect proteins that, generally, do not hold a net charge and undergo, upon interaction with their affinity ligands, conformational changes that largely consist of dielectric rearrangements. Moreover, with an EGOFET the overall relative change in I_D upon binding can be decoupled into the dielectric and electrostatic changes associated with C and V_T, respectively.[32,33]

It is also important to outline that, for the capacitive-coupling to hold, no stationary redox reactions have to take place at the gate and semiconductor interfaces. As already highlighted, from a modelling point of view, the resistance in parallel to C_G and C_{OSC} has to be sufficiently high in order to obtain a negligible gate leakage current, I_G. Indeed, when an electronic current flows through the gate, a FET behaves like a leaky transistor; the charge separation of the gating capacitance is neutralized, no capacitive-coupling exists anymore and the field-effect is lost. To keep I_G sufficiently low (at least three orders of magnitude lower than I_D), the electrochemical potential of any redox reaction does not have to fall in the V_G spanned range. Eventually, no Faradaic electronic current flows through the dielectric electrolyte and the transfer and output characteristics, measured in the forward and reverse scan, show no cyclic voltammetric characteristic peaks and hysteretic behaviour.

The capacity-coupling between C_{BIO} and the FET-channel in EGOFETs controls the sensing process as shown by the transfer-characteristics (I_D *vs.* V_G at fixed V_D) measured upon binding. In **Figure 7a** a current decrease and a V_T shift towards more negative values is measured upon exposure of the bio-functionalized gate to increasing concentrations of the biomarker. In this case an immunometric reaction is involved with no electrochemical processes occurring, as in the other EGOFETs proposed before. More relevantly, the I_D fractional change upon binding (**Figure 7b**) evidences that the sensing response scales with

the concentration only beyond the threshold voltage, while no correlation exists for I_G (**Figure 7c**), that is three orders-of-magnitude lower than I_D. Such evidences prove that the I_D current, being the only one modulated by C_{BIO} and amplified beyond V_T, enables the highly sensitive capacitively-coupled FET-transduction of the changes occurring in the bio-layer upon binding.

4.2 The hydrogen bonding network

The core of a bioelectronic EGOFET sensor is the bio-layer of recognition-elements; in *SiMoT* this is the SAM, schematically depicted in **Figure 7d**. It comprises a mixed SAM of carboxylic terminated alkanethiols (chem-SAM)[76] binding 10^{12} capturing-antibodies (anti-Immunoglobulin-G, anti-IgG) forming the bio-SAM. In the chem-SAM the hydrogen bondings (H-bonds), highlighted by red-arrows, connect two neighbouring chains and form an electrostatic network that virtually connects all the chains. The resultant dipole-moment modifies the gate work-function,[36] that causes a V_T shift. When the bio-SAM is physisorbed directly on the gate (no chem-SAM is present) an aM limit-of detection is reached at most with EG-FETs.[36,38] This means that 10^3 molecule are sensed and not just one molecule. Moreover, if no hydrogen bonding network is present, the sensing is lost.[36] Hence, the role of the H-bonding network is critical to reach single-molecule-sensing.[38] Molecular dynamic simulations of the dipoles associated with the H-bonds have been engaged to get insights into this phenomenon and are shown as arrows in **Figure 7e**. The gating-field makes the H-bond-network more ordered and stable,[36] while the θ angle between the chain-backbones and the gating-field (**Figure 7d**) decreases. It is assumed that, upon binding of a single biomarker to one of the 10^{12} recognition-elements, an energy release generates a local-disorder in the network. This is simulated by a permanent loss of the few H-bonds included into the red circle in **Figure 7f**. Apparently, the defect generates a completely different pattern of dipole-moments and, hence, the gate work-function changes appreciably. Most relevantly, the area

affected by the change largely exceeds that of the defect. Therefore, the H-bonding network in the field activates electrostatic-collective-interactions that propagate the initial defect generated by the single-affinity-binding. As a result, this changes the work function in a large area thus generating an amplification of the sensing signal. This was also supported by an analytical model based on Poisson statistics that gives an excellent reproduction of the experimental sensing dose curves and supports the model of the H-bonding network enabling the propagation of the single binding event effect to wider electrostatic domains.[36,37]

Interestingly, also in the ultrasensitive chiral FET discussed in Figure 5d, the carbonyl groups and amino groups of the Im+-Ph-β-CD are seen as possible forming an H-bonding between adjacent recognition elements, forming a network as well. Eventually, inclusion energy of Phe and one Im+-Ph-β-CD molecule could be transferred to its neighbors and propagate in the whole sensing layer through the H-bonding network to accomplish signal amplification.

5. Organic Electrochemical Transistor sensors

5.1 OECTs as biosensors of electroactive species

A great deal of published papers on organic FET biosensors are based on the OECT configuration[77–83] and among those the large majority is engaged with the detection of redox species such as for instance glucose,[84] gallic acid,[85] dopamine[86] and uric acid.[87] Another quite ample section of OECTs are engaged for selective ion detection.[88–91] In this respect, they can be considered complementary to the EGOFETs that usually sense species that are not electroactive by using ion-impermeable electronic channel materials. At the same time, it is worth to note that the mere electrochemical detection of the elicited species can return lower LODs. In fact, for glucose a LOD of 0.1 μM has been reported,[92] for gallic acid the LOD is 10.7 nM,[93] for dopamine is 0.1 nM,[94] and for uric acid is 0.12 μM.[93] Moreover, an EGOFET detecting dopamine at lower concentration,[31] than an OECT has been reported, while a capacitive-coupled OECT has been proven to detect at the aM limit.[35]

As already anticipated EGOFETs have been proposed only as potentiometric sensors while OECTs have been proposed both as amperometric and potentiometric sensors. The working operation conditions of OECTs detecting redox active species, though, are sometimes set in a way that it not straightforward to sort them unequivocally into one of these two categories. Such an occurrence becomes critical when the measured I_D current has to be used for a quantitative analysis as it is not clear if the right conditions for the application of either Equation 1a or Equation 1b are set. With the aim of elucidating this point, an overview of a selection of OECT bioelectronic sensors performances in detecting electroactive species is given in **Table 3**.

Table 3. Selected typical examples of OECT detecting electrochemical species

Analyte / marker	Gate electrode	Gate area (mm^2)	Channel area (mm^2)[a)]	Electrolyte	Ep (V vs Ag/AgCl)	Linearity range	LOD	LOQ	REF
Gallic acid (GA)	Au/MWNT-PDDA	9	1.2	PBS (pH= 7.4)	GA Epa: 0.63 and 0.86	1- 10 μM	10 nM	N.A.	[85]
Dopamine (DA)	Pt	N.A.	0.6	PBS (pH= 7.2)	DA Epa: 0.58	0.5 - 1000 nM	5 nM[b)]	N.A.	[86]
Glucose (Glu)	Pt/Gox/Chit./Pt_NPs	20	1.2	PBS (pH= 7.2)	H_2O_2 Epa: 0.6	0.005- 5 μM	5 nM[b)]	N.A.	[84]
Ascorbic acid (AA)	PEDOT:PSS	9	90	PBS (pH= 7.5)	AA Epa: 0.34	0.2- 0.8 mM	70 μM	N.A.	[87]
Uric Acid (UA)	PEDOT:PSS	9	90	PBS (pH= 7.5)	UA Epa: 0.46	0.04- 0.4 mM	20 μM	N.A.	[87]
Dopamine (DA)	PEDOT:PSS	9	90	PBS (pH= 7.5)	DA Epa: 0.40	0.025- 0.1 mM	6 μM	N.A.	[87]
Lactate	PEDOT:PSS/PVA/Fc-branched chitosan-LOx	0.25	0.01	PBS	Fc-chitosan Epa: 0.25 Epc: 0.15	0.1- 2 mM	N.A.	50 μM	[79]
Glucose (Glu)	PEDOT:PSS/PVA/Fc-branched chitosan-GOx	0.25	0.01	PBS	(Fc-chitosan) Epa: 0.25 Epc: 0.15	0.02 - 1 mM	N.A.	10 μM	[79]
Cholesterol	PEDOT:PSS/PVA/Fc-branched chitosan- ChOx	0.25	0.01	PBS	(Fc-chitosan) Epa: 0.25 Epc: 0.15	0.01 - 0.7 mM	N.A.	10 μM	[79]

[a)] Channel material: PEDOT:PSS, [b)] Lowest detected concentration

It can be first noticed that their performance level assessment returns best LODs or lowest detected concentrations that reach the nM level. In **Figure 8** two recently published examples of PEDOT-PSS OECTs detecting electroactive species are shown. The OECT device in the top panel (**Figure 8a** – **Figure 8c**) features a PEDOT-PSS OECT for the detection of 3,4,5-trihydroxybenzoic acid or gallic acid (Figure 8a).[85] This redox active species serves as a reference compound for the total polyphenol content and can be used to mimic the assay of anti-free-radical compounds. To this end, the Au gate electrode is functionalized with a nanocomposite of poly(diallyl dimethyl ammonium chloride) (PDDA) and multi-wall carbon nanotubes (MWNT), to enhance the performance of the sensor. Electrochemical cyclic voltammetry experiments show that the presence of the nanomaterials increase the electrocatalytic activity of the gold surface returning a higher faradic current. The sensing principle is based on the direct electro-oxidation of gallic acid that releases two electrons and generates a Faradic current into the gate electrode. The Authors underline that, due to the Faradaic current generation, the electrochemical potential of the gate changes and this shifts the OECT V_T. The Authors also propose a diagram (**Figure 8b)** of the potential drop between the gate and the channel of the OECT, before and after the addition of gallic acid in the PBS solution. In **Figure 8c** the I_D transient currents at increasing gallic acid concentration in PBS solution are measured. The inset shows that the noise level, taken as the average signal of the current and a LOD of 10 nM is computed. A comparison with a standard amperometric electrochemical detection is offered showing that, between 0.4 V and 0.6 V *vs.* the saturated calomel reference electrode, Faradaic currents can be measured. However, the transient I_D curve is measured at V_G = 0.6 V and the reference potential seems to be V_S (common-source configuration) this time. Moreover, while the OECT seems to be ranked as a potentiometric biosensor (a shift in V_T is addressed), it is not clear if the zero-current potential rule can be considered satisfied given that likely an electrochemical reaction, with the associated electronic current flux, is steadily occurring during the OECT measurement.

The second OECT discussed encompasses a PEDOT-PSS biofunctionalized surface (**Figure 8d**). Here an electrochemically driven OECTs is proposed for the enzymatic sensing of glucose, lactate and cholesterol.[79] The OECT is made of PEDOT-PSS on gold electrodes with the gate electrode serving as sensing element. To covalently attached the enzyme on the Au / PEDOT-PSS gate surface, the polymer is blend with polyvinyl alcohol (PVA) that provides the hydroxyl anchoring groups. The relevant enzyme (glucose-oxidase, lactate-oxidase or cholesterol oxidase) is attached to the gate through a ferrocene-branched chitosan SAM. The ferrocene/ferricenium ion couple serves also as a mediator and the cyclic voltammogram of the gate electrode shows that a large Faradaic current can be measured when the enzyme is attached to the gate and 10 mM of glucose is added (**Figure 8e**). In this case the OECT is operated as an amperometric sensor where the mediator is not H_2O_2 (Figure 1e) but ferrocene that oxidises at lower anodic potentials (**Figure 8f**). The calibration curves derived from the chronoamperometric response of the OECTs after successive additions of increasing concentrations of glucose is shown in **Figure 8g**. Upon addition of a sample containing the analyte of interest, an enzymatic reaction occurs, the enzyme is reduced and cycles back via the ferrocene/ferricenium couple which mediates electron transfer between the redox enzyme and the PEDOT-PSS gate electrode, due to its low oxidation potential. The measured LOQs are of the order of μM and the platform is integrated with a simple pumpless poly(dimethylsiloxane) (PDMS)-based microfluidic for the possible realization of point-of-care devices. One observation that can be made is that, while a chronoamperometric measurement is performed, the dependence of the I_D current measured is not linear but logarithmic with [c]. It is hence not clear if the gathered data should comply with Equation 1a or Equation 1b for quantification purposes.

The questions risen call for a deepening into the OECT sensing mechanisms and the differences that can be found with more standard electrochemical detections, particularly of electroactive species.

5.2 Discussion on Electrochemical transistors sensing mechanism

As already pointed out, the capacitive-coupling illustrated in Figure 2c, involving either a 2D or 3D capacitances, does not reflect inherently different device operational regimes. Rather, they echo the different chemical affinity between the channel material and the electrolyte.

This means that, provided the zero-potential rule is complied with, both EGOFETs and OECTs can be operated as potentiometric biosensors. The $\Delta\Phi$ potential shift upon sensing is given by Equation 1a and it reflects into I_D through the analytical equations given in Section 4.1. The enhancement of the signal, compared to electrochemical potentiometric or capacitance measurements, is associated with the capacitive-coupling between the bio-layer and the electronic channel that originate an I_D current enhanced by the transconductance of the FET device. Device operational and materials parameters can be tuned to maximise this effect. In the potentiometric operational regime, while the enhanced I_D clearly shifts with the concentration of the detected species, no dependence of I_G on the analyte concentration is measured. This occurs simply because I_G does not result from the capacitive coupling with the layer where the binding of the analyte occurs (Figure 7b and Figure 7c). Such an occurrence applies directly to the sensing of affinity binding interactions (Figure 1c and Figure 1b), while for the sensing involving electrochemical selective interaction (Figure 1e) the situation can be trickier. Indeed, potentiometric electrochemical detections of metabolites has been successfully proposed but the zero-current voltage condition imposes that the redox reaction extinguishes generating, for instance, a stable change in the electrolyte pH or at the bio-

functionalized interface, so as no transient electronic or ionic current flows during the potentiometric measurement.

A conceptual difference exists when the OECT operates in the amperometric mode which requires the involvement of an electrochemical reaction. To properly understand this aspect, it is worth to dwell into the electronic mechanisms in a redox reaction. In **Figure 9a** the alignment of the electrochemical potentials (E_0) or equivalently the Fermi Levels (E_F) of a PEDOT-PSS[95] or of an Au[96] electrode with that of the $Fe(CN)_6^{4-}$ / $Fe(CN)_6^{3-}$ redox couple, is illustrated. The alignment is presented versus the vacuum level by knowing that the E_0 / E_F of the Ag/AgCl (KCl sat.) electrode *vs.* vacuum is -4.7 eV.[97] The work functions of Au and PEDOT-PSS (in its high doped state) are apparently very similar. The Fe^{II} oxidation to Fe^{III} is also illustrated showing that, when the Au or the PEDOT-PSS electrodes are driven by an external bias at a sufficiently anodic potential, electrons from Fe^{II} can find free states in the Au or in the PEDOT-PSS electrode conduction band, and the oxidation process to Fe^{III} can take place. An electrochemical-cell is shown (**Figure 9b**), along with the oxidation reaction of Fe^{II} turning into Fe^{III} (red-arrow). When the external bias sets the working electrode at the E_0 of the redox species, an electronic Faradaic-current starts and it would be transient if not sustained by a second reaction, involving an electron withdrawal from the second electrode so that the circuit is closed by Ag^{I} turning into Ag^{0} (blue-arrow). In a standard electrochemical cell, the latter reaction has a fixed make-up with a continuous supply of reagents and a steady Faradaic-current flowing through it, so that its electrochemical potential is constant and can serve as reference.[47] Indeed, in the presence of a Faradaic-current, the reference electrode is essential as it keeps the potential in the solution fixed, regardless of the current intensity flowing. The channel-material, being also redox-active, can act as a mediator.[98] In fact, if the Au electrode is covered by a redox active film such as PEDOT-PSS, an electrochemical reaction can still take place at this electrode particularly when the electrochemical potentials of the redox species and that of the mediator membrane are close. This is indeed the case for

the PEDOT-PSS and the $Fe(CN)_6^{4-}$ / $Fe(CN)_6^{3-}$ redox couple as it seen in Figure 9a and it is confirmed in the experiment proposed in **Figure 9c.** Here a comparison between the Au and the Au / PEDOT-PSS interface to measure the cyclic voltammetry of Fe^{II} / Fe^{III} is proposed. As it can be seen, the anodic (E_{pa}) and cathodic (E_{pc}) peaks fall at the same potential and, if the low capacitance contribution to the total current is subtracted (**Table 4**), roughly the same Faradaic current can be measured.

Table 4: Electrochemical data (anodic peak potential E_{pa}, cathodic peak E_{pc}, and peak separation ΔE_p,) and charge (C) measured for the bare Au and Au / PEDOT- PSS in 1 mM $K_4[Fe(CN)_6] \cdot 3H_2O$ in 0.1M KCl

	E_{pa} (mV)	E_{pc} (mV)	ΔE_p (mV)	Capacitive Charge (C)	Faradaic Charge (C)
Au /Kapton	284	182	102	1.56E-06	2.42E-05
PEDOT: PSS/Au/Kapton	282	188	94	1.41E-05	5.40E-05

It has been shown that the Faradaic current at a PEDOT-PSS electrode is independent of the film thickness (**Figure 10a**)[60] Further on it was demonstrated that the density of percolation paths for the electronic transport within the PEDOT-PSS electrode dictates the overall rate of electron transfer at the electrolyte polymer electrode interface. This implies that the oxidation of ferrocyanide (Fe^{II}) to ferricyanide (Fe^{III}) occurs via a percolation path of reduction of the PEDOT-PSS with a subsequent lowering of its conductivity. Such an occurrence is illustrated in **Figure 10b**.

An OECT detecting the redox species mimicking an enzymatic-selective-reaction (Figure 1e) is shown in **Figure 10c**. Relevantly Ag/AgCl (KCl sat.) is set as reference as in the electrochemical experiment. Since the device is operated as an amperometric sensor, V_G is set so that at the interface with the PEDOT-PSS the electrochemical potential of the Fe^{II}/ Fe^{III} redox couple is set. The oxidation (red-arrow) starts when V_G aligns with its electrochemical-potential *vs.* that of the reaction closing the circuit (blue-arrow) Ag/AgCl (KCl sat.) reference electrode. If the electrochemical-potentials are all aligned, at the corresponding V_G a

Faradaic-current I_G flows between the gate (reference electrode) and the source. Importantly, the PEDOT-PSS acts essentially only as a mediator for the electron transfer. The ionic charging is also stoichiometrically related to the net transfer of electronic charge. This results in a net change of the electrochemical potential of the source which modulates the I_D current flowing between the source and the drain. Indeed, the capacitance charging of PEDOT-PSS is not dominating over the Faradaic one (Table 4). Similarly, to a homologous electrochemical amperometric sensor, no capacity-coupling is installed because when an electronic-current leaks through the gate, from a modelling point of view, the capacitance C_G is shorted by a small parallel resistance R_G and, as a result, C_G can be neglected. Under the assumption that the Faradaic-current leaks also through the channel material, C_{OSC} and the field-effect are lost too. It is therefore not clear if an enhancement is in place to justify the use of an amperometric OECT over an equivalent amperometric electrochemical biosensor. A comparison between the two approaches can be carried out but it must involve operating the two biosensors using exactly the same bias, geometrical factors and scan rates. Alternatively, the relative changes of the currents should be presented.

To better elucidate the concept, the study of the I_D *vs.* I_G current in an experiment involving the OECT operated as in Figure 10c, was performed. Specifically, the OECT was operated in KCl 0.1 M added with 1 mM and 10 mM of $K_4[Fe(CN)_6] \cdot 3H_2O$. The gate was swept from -0.4 V to 0.4 V and the I_D-V_G transfer curves were recorded at three different constant drain voltages, V_D = - 0.4 V, V_D = - 0.2 V, V_D = 0 V. The results show two key aspects: I) I_G scales with the ferrocyanide concentration; II) at V_D = - 0.4 V, V_D = - 0.2 V, the relative variation of the I_D upon sensing addressed as $(\Delta I/I_0)_D$ was much lower than $(\Delta I/I_0)_G$ at all the ferrocyanide concentrations. As an instance: at V_G = - 0.12 V (highest transconductance), V_D = - 0.2 V, 1 mM ferrocyanide concentration $(\Delta I/I_0)_D$ = - 2 % while $(\Delta I/I_0)_G$ = - 35%. Under the same conditions but at 10 mM ferrocyanide concentration $(\Delta I/I_0)_D$ = - 5% while $(\Delta I/I_0)_G$ = - 274%.

This is a rather strong evidence that an OECT amperometric biosensor does not appear to outperform an equivalent amperometric electrochemical biosensor.

For the sake of completeness it is to be added that, if the gate electrode is a gold layer and not the reference electrode, the redox reaction can take place at the gate (maybe functionalized) until the Faradaic Cottrell current (Equation 1b), extinguishes. This changes the gate electrochemical potential that can be detected via a capacitively-coupled FET. However, due to the absence of the reference electrode, such a measurement cannot be considered for quantitative purposes, as the redox reaction is not carried out under the potential control necessary for the Cottrell to hold.

At variance, since in an amperometric device a current flows, a transistor that can amplify a current, and not a potential, should be used. In this respect a *resistive-coupling* instead of a capacity-coupling between the gate and the channel should be exploited. To this aim, a bipolar-junction-transistor could be considered,[99] as it is a paradigmatic example of current-amplifier. Indeed, the emitter-collector-current can be up to 10^2 larger than the base-one. An ionic-equivalent of a resistive-coupled device has been proposed,[100,101] and could be used as the basis to design an OECT as n-p/p-n electronic/ionic bipolar-junctions in series, so that I_D (equivalent to the emitter-collector-one) can transduce and amplify I_G (equivalent to the base-one). Alternatively, the redox-reaction should take place while I_D is not measure. Afterwards, provided the gate new electrochemical-state is stable, it can be assessed in a capacity-coupled configuration.

A last remark concerns the reference-electrode, necessary to keep the solution potential fixed when a Faradaic-current flows into the gate. Hence, it is mandatory needed to stably operate an amperometric driven OECT. However, reference-electrodes have not yet been successfully integrated in an electronic circuit,[102] and this drawback has impaired the commercialization of electrochemical-sensor-arrays. The need for such element can be less critical in capacity-coupling regimes as no I_G flows and, indeed, EGOFETs are generally stably operated with no

reference-electrode.[5,22,32–36,38] Indeed, even with an EGOFET more stable potentials are measured with the use of a reference electrode.

6. Conclusions

The field of organic bioelectronic sensors is critically reviewed by addressing, for the first time in a systematic fashion, both the Electrolyte-Gated Organic Field-Effect Transistors (EGOFETs) and Organic ElectroChemical Transistors (OECTs) configurations. Materials properties and devices structures are rationalized to unambiguously attribute a given bioelectronic sensor to the well assessed and long-time studies potentiometric and amperometric electrochemical biosensor categories. This is relevant to choose the most suitable materials, devices structures and operating condition that enable to correctly detect and quantify of the detected species. It also describes how to reliably characterize the biosensors figures of merit and performance level. The final aim is to provide the community working on organic bioelectronic sensors with a comprehensive set of tools that will help to take full advantage of the processes that enhance the sensing response enabling extremely high-performance level resulting in ultimate sensitivity, selectivity and fast response.

Experimental

Electrodes fabrication and cyclic voltammetry measurements

Gold disk electrodes (~ 0.2 cm^2) were photo-lithographically defined on a Kapton foil substrate. Gold was e-beam evaporated (50 nm) using titanium as adhesion promoting layer (5 nm). After the electrodes cleaned by sonication in acetone (10 min) and isopropanol (10 min) then they were rinsed with HPLC water and dried with nitrogen.

For the preparation of the PEDOT-PSS on Au disk electrodes (~ 0.2 cm^2), the semiconductor solution was spin coated at 500 rpm for 10 s and at 2000 rpm for 50 s. The film was subsequently

baked at 140 °C for 1 h and immersed in deionized water to remove any excess of low-molecular-weight compounds. The solution was prepared according to the following procedure: 20 ml of aqueous dispersion of poly(3,4-ethylenedioxythiophene): poly(styrene sulfonic acid) PEDOT-PSS (PH-500 from Heraeus Clevios GmbH) and 1 ml of Dimethyl sulfoxide (DMSO) were mixed and sonicated before spin coating.

For the electrochemical measurements the bare Au/Kapton and PEDOT-PSS/Au/Kapton disk electrodes slide were used as a working electrodes (WE), while Au lamina sheet was used as counter electrode (CE) and Ag/AgCl (KCl sat.) as reference (RE). All electrodes were directly connected to a CH Instrument Electrochemical Analyzer (Model CHI1230B). The anodic current was set positive. Cyclic voltammetry was carried out in 0.1 M potassium chloride (KCl, Fluka, puriss p.a.) and in presence of 1 mM potassium ferrocyanide $K_4[Fe(CN)_6] \cdot 3H_2O$ (Sigma Aldrich, 98.5%) in 0.1 M KCl supporting electrolyte with an applied potential in the range of - 0.2 to + 0.6V., scan rate 0.1 Vs^{-1}. The Ag/AgCl (KCl sat.) was measured at - 46.4 mV *vs.* saturated calomel electrode (SCE).

OECT device fabrication and I-V electrical measurements

Glass slides were cleaned by sonication in acetone, isopropyl alcohol, and deionized water, followed by drying and UV ozone cleaning. 100 nm thick gold source/drain parallel contacts were evaporated through a shadow mask defining the device channel length. An adhesion layer of 5 nm of chromium was previously deposited. The PEDOT- PSS film was deposited as mentioned above. A 1.8 μm AZ1518 positive photoresist purchased form Microchemicals GmbH and used as received was spin coated and photolithographically patterned on top of electrodes to avoid unwanted electrochemical reaction of the gold electrodes. A cell was glued around the channels area and was filled with 900 μL of 0.1M KCl or of 1 and 10 mM, $K_4[Fe(CN)_6] \cdot 3H_2O$ in 0.1M KCl. The area of PEDOT - PSS exposed to the electrolyte solution was approximately 0.0018 cm^2. Ag/AgCl (KCl sat.) was used as gate electrode.

OECTs were characterized with Keithley 4200 SCS semiconductor parameter analyser. The gate was swept from -0.4 V to 0.4 V with a step 5 mV with a scan rate of 0.1 Vs^{-1}. I-V curves were recorded at three different constant drain voltages, V_D = - 0.4 V, V_D = - 0.2 V, V_D = 0 V.

Acknowledgements

We are thankful to Prof. Beatrice Fraboni and her group for useful discussions on the OCETs functional mechanisms. The following grants are acknowledged for partial financial support: Future in Research – *FLOW:* Dispositivi EGOFET flessibili a bassa tensione per la sicurezza in campo alimentare (ML5BJ85); Future In Research – *BEND*: Biosensori elettronici intelligenti per la diagnosi precoce di malattie neurodegenerative (B164PG8); H2020 - Electronic Smart Systems - *SiMBiT:* Single molecule bio-electronic smart system array for clinical testing (Grant agreement ID: 824946); MIUR PON - *e-DESIGN*: Combination of Design, Electronics and Multifunctional Materials for New Aesthetic Components (ARS01_01158). CSGI is also acknowledged for partial financial support.

References

[1] M. Kaisti, *Biosens. Bioelectron.* **2017**, *98*, 437.

[2] P. Bergveld, *Sens. Actuators B Chem.* **2003**, *88*, 1.

[3] S. Caras, J. Janata, *Anal. Chem.* **1980**, *52*, 1935.

[4] R. B. M. Schasfoort, P. Bergveld, R. P. H. Kooyman, J. Greve, *Anal. Chim. Acta* **1990**, *238*, 323.

[5] C.-H. Chu, I. Sarangadharan, A. Regmi, Y.-W. Chen, C.-P. Hsu, W.-H. Chang, G.-Y. Lee, J.-I. Chyi, C.-C. Chen, S.-C. Shiesh, G.-B. Lee, Y.-L. Wang, *Sci. Rep.* **2017**, *7*, 5256.

[6] D.-J. Kim, H.-C. Park, I. Y. Sohn, J.-H. Jung, O. J. Yoon, J.-S. Park, M.-Y. Yoon, N.-E. Lee, *Small* **2013**, *9*, 3352.

[7] S. Cheng, K. Hotani, S. Hideshima, S. Kuroiwa, T. Nakanishi, M. Hashimoto, Y. Mori, T. Osaka, *Materials* **2014**, *7*, 2490.

[8] D. M. Rissin, C. W. Kan, T. G. Campbell, S. C. Howes, D. R. Fournier, L. Song, T. Piech, P. P. Patel, L. Chang, A. J. Rivnak, E. P. Ferrell, J. D. Randall, G. K. Provuncher, D. R. Walt, D. C. Duffy, *Nat. Biotechnol.* **2010**, *28*, 595.

[9] L. Torsi, G. M. Farinola, F. Marinelli, M. C. Tanese, O. H. Omar, L. Valli, F. Babudri, F. Palmisano, P. G. Zambonin, F. Naso, *Nat. Mater.* **2008**, *7*, 412.

[10] S. P. White, C. D. Frisbie, K. D. Dorfman, *ACS Sens.* **2018**, *3*, 395.

[11] H. U. Khan, M. E. Roberts, O. Johnson, R. Förch, W. Knoll, Z. Bao, *Adv. Mater.* **2010**, *22*, 4452.

[12] M.-J. Spijkman, J. J. Brondijk, T. C. T. Geuns, E. C. P. Smits, T. Cramer, F. Zerbetto, P. Stoliar, F. Biscarini, P. W. M. Blom, D. M. de Leeuw, *Adv. Funct. Mater.* **2010**, *20*, 898.

[13] M. Demelas, S. Lai, G. Casula, E. Scavetta, M. Barbaro, A. Bonfiglio, *Sens. Actuators B Chem.* **2012**, *171–172*, 198.

[14] L. Torsi, M. Magliulo, K. Manoli, G. Palazzo, *Chem. Soc. Rev.* **2013**, *42*, 8612.

[15] S. Lai, M. Demelas, G. Casula, P. Cosseddu, M. Barbaro, A. Bonfiglio, *Adv. Mater.* **2013**, *25*, 103.

[16] S. P. White, K. D. Dorfman, C. D. Frisbie, *Anal. Chem.* **2015**, *87*, 1861.

[17] I. Gualandi, M. Marzocchi, A. Achilli, D. Cavedale, A. Bonfiglio, B. Fraboni, *Sci. Rep.* **2016**, *6*, 33637.

[18] W. Shi, Y. Zheng, A. D. Taylor, J. Yu, H. E. Katz, *Appl. Phys. Lett.* **2017**, *111*, 043301.

[19] B. Piro, D. Wang, D. Benaoudia, A. Tibaldi, G. Anquetin, V. Noël, S. Reisberg, G. Mattana, B. Jackson, *Biosens. Bioelectron.* **2017**, *92*, 215.

[20] M. Yilmaz, E. Babur, M. Ozdemir, R. L. Gieseking, Y. Dede, U. Tamer, G. C. Schatz, A. Facchetti, H. Usta, G. Demirel, *Nat. Mater.* **2017**, *16*, 918.

[21] M. Berggren, A. Richter-Dahlfors, *Adv. Mater.* **2007**, *19*, 3201.

[22] L. Kergoat, L. Herlogsson, D. Braga, B. Piro, M.-C. Pham, X. Crispin, M. Berggren, G. Horowitz, *Adv. Mater.* **2010**, *22*, 2565.

[23] L. H. Jimison, S. A. Tria, D. Khodagholy, M. Gurfinkel, E. Lanzarini, A. Hama, G. G. Malliaras, R. M. Owens, *Adv. Mater.* **2012**, *24*, 5919.

[24] S. H. Kim, K. Hong, W. Xie, K. H. Lee, S. Zhang, T. P. Lodge, C. D. Frisbie, *Adv. Mater.* **2013**, *25*, 1822.

[25] F. Pettersson, R. Österbacka, J. Koskela, A. Kilpelä, T. Remonen, Y. Zhang, S. Inkinen, C.-E. Wilén, R. Bollström, M. Toivakka, A. Määttänen, P. Ihalainen, J. Peltonen, *MRS Commun.* **2014**, *4*, 51.

[26] F. Pettersson, T. Remonen, D. Adekanye, Y. Zhang, C.-E. Wilén, R. Österbacka, *ChemPhysChem* **2015**, *16*, 1286.

[27] T. Someya, Z. Bao, G. G. Malliaras, *Nature* **2016**, *540*, 379.

[28] D. T. Simon, E. O. Gabrielsson, K. Tybrandt, M. Berggren, *Chem. Rev.* **2016**, *116*, 13009.

[29] C. Pitsalidis, A.-M. Pappa, M. Porel, C. M. Artim, G. C. Faria, D. T. Duong, C. A. Alabi, S. Daniel, A. Salleo, R. M. Owens, *Adv. Mater.* **2018**, *30*, 1803130.

[30] J. Rivnay, S. Inal, A. Salleo, R. M. Owens, M. Berggren, G. G. Malliaras, *Nat. Rev. Mater.* **2018**, *3*, 17086.

[31] S. Casalini, F. Leonardi, T. Cramer, F. Biscarini, *Org. Electron.* **2013**, *14*, 156.

[32] M. Y. Mulla, E. Tuccori, M. Magliulo, G. Lattanzi, G. Palazzo, K. Persaud, L. Torsi, *Nat. Commun.* **2015**, *6*, 6010.

[33] K. Manoli, M. Magliulo, M. Y. Mulla, M. Singh, L. Sabbatini, G. Palazzo, L. Torsi, *Angew. Chem. Int. Ed.* **2015**, *54*, 12562.

[34] S. J. Park, O. S. Kwon, S. H. Lee, H. S. Song, T. H. Park, J. Jang, *Nano Lett.* **2012**, *12*, 5082.

[35] E. Macchia, P. Romele, K. Manoli, M. Ghittorelli, M. Magliulo, Z. M. Kovács-Vajna, F. Torricelli, L. Torsi, *Flex. Print. Electron.* **2018**, *3*, 034002.

[36] E. Macchia, K. Manoli, B. Holzer, C. Di Franco, M. Ghittorelli, F. Torricelli, D. Alberga, G. F. Mangiatordi, G. Palazzo, G. Scamarcio, L. Torsi, *Nat. Commun.* **2018**, *9*, 3223.

[37] *Nature* **2018**, *560*, 413.

[38] E. Macchia, A. Tiwari, K. Manoli, B. Holzer, N. Ditaranto, R. A. Picca, N. Cioffi, C. Di Franco, G. Scamarcio, G. Palazzo, L. Torsi, *Chem. Mater.* **2019**.

[39] E. Macchia, K. Manoli, B. Holzer, C. Di Franco, R. A. Picca, N. Cioffi, G. Scamarcio, G. Palazzo, L. Torsi, *Anal Bioanal Chem* **2019**, in press.

[40] T. Cramer, A. Campana, F. Leonardi, S. Casalini, A. Kyndiah, M. Murgia, F. Biscarini, *J. Mater. Chem. B* **2013**, *1*, 3728.

[41] G. Palazzo, D. De Tullio, M. Magliulo, A. Mallardi, F. Intranuovo, M. Y. Mulla, P. Favia, I. Vikholm-Lundin, L. Torsi, *Adv. Mater.* **2015**, *27*, 911.

[42] P. Seshadri, K. Manoli, N. Schneiderhan-Marra, U. Anthes, P. Wierzchowiec, K. Bonrad, C. Di Franco, L. Torsi, *Biosens. Bioelectron.* **2018**, *104*, 113.

[43] M. Magliulo, D. De Tullio, I. Vikholm-Lundin, W. M. Albers, T. Munter, K. Manoli, G. Palazzo, L. Torsi, *Anal. Bioanal. Chem.* **2016**, *408*, 3943.

[44] C. Suspène, B. Piro, S. Reisberg, M.-C. Pham, H. Toss, M. Berggren, A. Yassar, G. Horowitz, *J. Mater. Chem. B* **2013**, *1*, 2090.

[45] Paolo Romele, Matteo Ghittorelli, Zsolt Miklós Kovács-Vajna, Fabrizio Torricelli, *Nat. Commun.* **2019**, under review.

[46] B. Piro, G. Mattana, S. Zrig, G. Anquetin, N. Battaglini, D. Capitao, A. Maurin, S. Reisberg, *Appl. Sci.* **2018**, *8*, 928.

[47] A. J. Bard, L. R. Faulkner, *Electrochemical Methods: Fundamentals and Applications, 2nd Edition*; 2nd ed.; Wiley: New York, 2001.

[48] K. Melzer, M. Brändlein, B. Popescu, D. Popescu, P. Lugli, G. Scarpa, *Faraday Discuss.* **2014**, *174*, 399.

[49] Biomarkers Definitions Working Group, *Clin. Pharmacol. Ther.* **2001**, *69*, 89.

[50] M. J. Selleck, M. Senthil, N. R. Wall, *Biomark. Insights* **2017**, *12*, 1177271917715236.

[51] M. Thompson, S. L. R. Ellison, R. Wood, *Pure Appl. Chem.* **2002**, *74*, 835.

[52] X.-P. He, X.-L. Hu, T. D. James, J. Yoon, H. Tian, *Chem. Soc. Rev.* **2017**, *46*, 6687.

[53] G. den Boef, A. Hulanicki, *Pure Appl. Chem.* **2009**, *55*, 553.

[54] D. R. Thévenot, K. Toth, R. A. Durst, G. S. Wilson, *Anal. Lett.* **2001**, *34*, 635.

[55] A. R. Hillman, *J. Solid State Electrochem.* **2011**, *15*, 1647.

[56] H. Sirringhaus, P. J. Brown, R. H. Friend, M. M. Nielsen, K. Bechgaard, B. M. W. Langeveld-Voss, A. J. H. Spiering, R. A. J. Janssen, E. W. Meijer, P. Herwig, D. M. de Leeuw, *Nature* **1999**, *401*, 685.

[57] D. Alberga, G. F. Mangiatordi, L. Torsi, G. Lattanzi, *J. Phys. Chem. C* **2014**, *118*, 8641.

[58] K. Manoli, L. M. Dumitru, M. Y. Mulla, M. Magliulo, C. D. Franco, M. V. Santacroce, G. Scamarcio, L. Torsi, *Sensors* **2014**, *14*, 16869.

[59] C. M. Palumbiny, F. Liu, T. P. Russell, A. Hexemer, C. Wang, P. Müller-Buschbaum, *Adv. Mater.* **2015**, *27*, 3391.

[60] K. Wijeratne, U. Ail, R. Brooke, M. Vagin, X. Liu, M. Fahlman, X. Crispin, *Proc. Natl. Acad. Sci.* **2018**, *115*, 11899.

[61] H. S. White, G. P. Kittlesen, M. S. Wrighton, *J. Am. Chem. Soc.* **1984**, *106*, 5375.

[62] A. V. Volkov, K. Wijeratne, E. Mitraka, U. Ail, D. Zhao, K. Tybrandt, J. W. Andreasen, M. Berggren, X. Crispin, I. V. Zozoulenko, *Adv. Funct. Mater.* **2017**, *27*, 1700329.

[63] J. Rivnay, P. Leleux, M. Ferro, M. Sessolo, A. Williamson, D. A. Koutsouras, D. Khodagholy, M. Ramuz, X. Strakosas, R. M. Owens, C. Benar, J.-M. Badier, C. Bernard, G. G. Malliaras, *Sci. Adv.* **2015**, *1*, e1400251.

[64] A. Al Baroot, A. Alshammari, M. Grell, *Thin Solid Films* **2019**, *669*, 665.

[65] A. Giovannitti, D.-T. Sbircea, S. Inal, C. B. Nielsen, E. Bandiello, D. A. Hanifi, M. Sessolo, G. G. Malliaras, I. McCulloch, J. Rivnay, *Proc. Natl. Acad. Sci.* **2016**, *113*, 12017.

[66] P. Lin, X. Luo, I.-M. Hsing, F. Yan, *Adv. Mater.* **2011**, *23*, 4035.

[67] N. M. Andoy, M. S. Filipiak, D. Vetter, Ó. Gutiérrez-Sanz, A. Tarasov, *Adv. Mater. Technol.* **2018**, *3*, 1800186.

[68] Y. Wu, X. Wang, X. Li, Y. Xiao, Y. Wang, *Chin. Chem. Lett.* **2019**.

[69] D. M. Rissin, D. R. Walt, *Nano Lett.* **2006**, *6*, 520.

[70] R. Iino, L. Lam, K. V. Tabata, Y. Rondelez, H. Noji, *Jpn. J. Appl. Phys.* **2009**, *48*, 08JA04.

[71] E. Engvall, P. Perlmann, *Immunochemistry* **1971**, *8*, 871.

[72] C.-M. Cheng, A. W. Martinez, J. Gong, C. R. Mace, S. T. Phillips, E. Carrilho, K. A. Mirica, G. M. Whitesides, *Angew. Chem. Int. Ed.* **2010**, *49*, 4771.

[73] S. Sorgenfrei, C. Chiu, R. L. Gonzalez Jr, Y.-J. Yu, P. Kim, C. Nuckolls, K. L. Shepard, *Nat. Nanotechnol.* **2011**, *6*, 126.

[74] B. Holzer, K. Manoli, N. Ditaranto, E. Macchia, A. Tiwari, C. Di Franco, G. Scamarcio, G. Palazzo, L. Torsi, *Adv. Biosyst.* **2017**, *1*, 1700055.

[75] E. Macchia, S. K. Sailapu, I. Merino-Jimenez, J. P. Esquivel, L. Sarcina, G. Scamarcio, S. D. Minteer, N. Sabaté, L. Torsi, *Biosens Bioelectron* **2019**, submitted.

[76] J. W. Lee, S. J. Sim, S. M. Cho, J. Lee, *Biosens. Bioelectron.* **2005**, *20*, 1422.

[77] G. Tarabella, C. Santato, S. Y. Yang, S. Iannotta, G. G. Malliaras, F. Cicoira, *Appl. Phys. Lett.* **2010**, *97*, 123304.

[78] R.-X. He, M. Zhang, F. Tan, P. H. M. Leung, X.-Z. Zhao, H. L. W. Chan, M. Yang, F. Yan, *J. Mater. Chem.* **2012**, *22*, 22072.

[79] A.-M. Pappa, V. F. Curto, M. Braendlein, X. Strakosas, M. J. Donahue, M. Fiocchi, G. G. Malliaras, R. M. Owens, *Adv. Healthc. Mater.* **2016**, *5*, 2295.

[80] E. Battista, V. Lettera, M. Villani, D. Calestani, F. Gentile, P. A. Netti, S. Iannotta, A. Zappettini, N. Coppedè, *Org. Electron.* **2017**, *40*, 51.

[81] M. Braendlein, A.-M. Pappa, M. Ferro, A. Lopresti, C. Acquaviva, E. Mamessier, G. G. Malliaras, R. M. Owens, *Adv. Mater.* **2017**, *29*, 1605744.

[82] A. M. Pappa, D. Ohayon, A. Giovannitti, I. P. Maria, A. Savva, I. Uguz, J. Rivnay, I. McCulloch, R. M. Owens, S. Inal, *Sci. Adv.* **2018**, *4*, eaat0911.

[83] I. Gualandi, E. Scavetta, F. Mariani, D. Tonelli, M. Tessarolo, B. Fraboni, *Electrochimica Acta* **2018**, *268*, 476.

[84] H. Tang, F. Yan, P. Lin, J. Xu, H. L. W. Chan, *Adv. Funct. Mater.* **2011**, *21*, 2264.

[85] C. Xiong, Y. Wang, H. Qu, L. Zhang, L. Qiu, W. Chen, F. Yan, L. Zheng, *Sens. Actuators B Chem.* **2017**, *246*, 235.

[86] H. Tang, P. Lin, H. L. W. Chan, F. Yan, *Biosens. Bioelectron.* **2011**, *26*, 4559.

[87] I. Gualandi, D. Tonelli, F. Mariani, E. Scavetta, M. Marzocchi, B. Fraboni, *Sci. Rep.* **2016**, *6*, 35419.

[88] P. Lin, F. Yan, H. L. W. Chan, *ACS Appl. Mater. Interfaces* **2010**, *2*, 1637.

[89] M. Sessolo, J. Rivnay, E. Bandiello, G. G. Malliaras, H. J. Bolink, *Adv. Mater.* **2014**, *26*, 4803.

[90] M. Ghittorelli, L. Lingstedt, P. Romele, N. I. Crăciun, Z. M. Kovács-Vajna, P. W. M. Blom, F. Torricelli, *Nat. Commun.* **2018**, *9*, 1441.

[91] F. Mariani, I. Gualandi, M. Tessarolo, B. Fraboni, E. Scavetta, *ACS Appl. Mater. Interfaces* **2018**, *10*, 22474.

[92] Y. Huang, X. Qin, Z. Li, Y. Fu, C. Qin, F. Wu, Z. Su, M. Ma, Q. Xie, S. Yao, J. Hu, *Biosens. Bioelectron.* **2012**, *31*, 357.

[93] Z. Liang, H. Zhai, Z. Chen, H. Wang, S. Wang, Q. Zhou, X. Huang, *Sens. Actuators B Chem.* **2016**, *224*, 915.

[94] J. Zou, S. Wu, Y. Liu, Y. Sun, Y. Cao, J.-P. Hsu, A. T. Shen Wee, J. Jiang, *Carbon* **2018**, *130*, 652.

[95] M. Y. Jo, S. J. Park, T. Park, Y. S. Won, J. H. Kim, *Org. Electron.* **2012**, *13*, 2185.

[96] Z. Chen, M. J. Lee, R. Shahid Ashraf, Y. Gu, S. Albert-Seifried, M. Meedom Nielsen, B. Schroeder, T. D. Anthopoulos, M. Heeney, I. McCulloch, H. Sirringhaus, *Adv. Mater.* **2012**, *24*, 647.

[97] J. Bisquert, P. Cendula, L. Bertoluzzi, S. Gimenez, *J. Phys. Chem. Lett.* **2014**, *5*, 205.

[98] L. Torsi, E. De Giglio, L. Sabbatini, P. G. Zambonin, *J. Electrochem. Soc.* **1994**, *141*, 2608.

[99] S. M. Sze, K. K. Ng, *Physics of semiconductor devices*; John wiley & sons, 2006.

[100] Z. Mousavi, A. Ekholm, J. Bobacka, A. Ivaska, *Electroanalysis* **2009**, *21*, 472.

[101] K. Tybrandt, K. C. Larsson, A. Richter-Dahlfors, M. Berggren, *Proc. Natl. Acad. Sci.* **2010**, *107*, 9929.

[102] S. Joo, R. B. Brown, *Chem. Rev.* **2008**, *108*, 638.

Figure 1. Bottom source and drain contacts bioelectronic field-effect transistor structures that are operated in an electrolyte. The layer of biological recognition elements integrated into the device structure to endow the device with selectivity can be either attached to the gate surface **(a)** or to the organic semiconductor interface **(b). (c)** A specific-capturing-antibody binding an antigen-biomarker and **(d)** a DNA probe binding a complementary DNA-genetic-biomarker, are sketched. **(e)** An enzyme (glucose-oxidase) selectively interacting, *via* an electrochemical reaction, with its substrate (glucose) is featured.

Figure 2. (**a**) top panel - Chemical structure of the ion impermeable poly(3-hexylthiophene-2,5-diyl) (P3HT) and the poly [2,5-bis(3-tetradecylthiophen-2-yl) thieno[3,2-b]thiophene] (PBTTT). These are two of the most used polythiophenes in organic electronics; bottom panel - schematic representation of the self-assembly of the P3HT chains in organic thin-films: thanks to the aliphatic moieties and the elevate regioregularity, the semiconductor assumes a lamellar structure with an elevate degree of hydrophobicity. The resulting film is not ion-permeable generating a 2D capacitance at the interface semiconductor/electrolyte. **(b)** Structure of the ion-permeable Poly(3,4-ethylenedioxythiophene) polystyrene sulfonate (PEDOT-PSS) channel material. Reproduced with permission.[60] Copyright 2018, National Academy of Sciences. (**c**) Cross-sectional view of an EGOFET sensor highlighting the charge double layers that forms when the ion-impermeable channel material is engaged. **(d)** Schematics of an OECT sensor, in the presence of a Faradaic current flowing into the organic semiconductor.

Figure 3. Typical EGOFET sensor with the biorecognition layer covalently attached to the gold gate surface: **(a)** the device structure evidencing the liquid gating solution and the gate electrode as well as the bio-sensing surface. **(b)** The chemical structure of the interface dipole

which is formed upon binding of dopamine to the biological recognition self-assembled monolayer on the gold surface. **(c)** cross-sectional view of the various layers of the device showing the electrostatic potential profiles and their coupling across interfaces. **(d)** Transfer characteristics measured at the different dopamine concentrations. Reproduced with permission.[31] Copyright 2013, Elsevier. **(e)** Schematic representation of a bioelectronic EGOFET immunosensor for procalcitonin (PCT) detection. The anti-PCT antibody is physisorbed on the P3HT surface (panel 1) followed by surface blocking with bovine serum albumin (BSA) to reduce nonspecific interaction (panel 2). The immunosensor is exposed to PCT (panel 3). **(f)** the electrical response is measured as the EGOFET transfer characteristics at different PCT concentrations. Reproduced with permission.[42] Copyright 2018, Elsevier.

Figure 4. (a) Typical structure of an EGOFET device capable to detect at the single molecule limit, the gold-gate area is $\sim 5 \cdot 10^{-1}$ cm^2 while the density of anti-Human-Immunoglobulin-G is $\sim 2 \cdot 10^{12}$ cm^{-2}. This device is addressed as *Single-Molecule with a large-Transistor* (SiMoT); Reproduced with permission.[36] Copyright 2018, Springer Nature. **(b)** Picture of the SiMoT device; Reproduced with permission.[37] Copyright 2018, Springer Nature. **(c)** Human-Immunoglobulin-G (H-IgG) curve in phosphate-buffer-saline solution in the 0-100 zM range is shown as the fractional change of I_D, $\Delta I/I_0$. The X-axis bars are the Poisson errors while Y-axis ones are the reproducibility errors. **(d)** Dose curve of Human-Immunoglobulin-G added into whole real bovine-blood-serum (red-squares) in the 0.6 zM - $6 \cdot 10^7$ zM range. In the control experiment Human-Immunoglobulin-M was used (black-circles) in please of the specific-recognition element anti-Human-Immunoglobulin-G used for the sensing. The continuous red-line is the result of the modelling based on Poisson-distribution-probability, suitable to account for single-binding-events. All the data points are the average over three replicates measured on different gates and different transistors. Error bars are taken as one standard deviation. Reproduced with permission.[36] Copyright 2018, Springer Nature.

Figure 5. (a) Electrolyte-gated FET bioelectronic-nose sensor based on plasma-treated bilayer graphene whose outmost surface is conjugated with a human olfactory receptors 2AG1 (hOR2AG1). **(b)** Picture detailing the bio-functionalized graphene FET-channel (region between source and drain contacts) whose are is ~ 10^{-2} cm^2. The density of hOR2AG1 receptors is ~ $5 \cdot 10^{11}$ cm^{-2}. **(c)** Responses as the fractional change of I_D, $\Delta I/I_0$, of the bioelectronic-nose upon exposure to different concentrations of the amyl-butylate odorant. The red-line is measured on an oxygen-plasma-treated graphene surface while the blue-line is relevant to an ammonia-plasma-treated surface. The black-trace is the response of a pristine graphene. Reproduced with permission.[34] Copyright 2012, American Chemical Society. **(d)** The device structure of a bottom gate FET where a β-cyclodextrin (β-CD) derivative - mono-6-deoxy-6-(1-allylimidazolium)-per(3,5-dimethyl)-phenylcarbamoylated-β-CD (Im^+-Ph-β-CD) - is deposited directly on a copper hexa-decafluoro-phthalocyanine (F_{16}CuPc) organic semiconducting layer. **(e)** Transient current changes upon exposure of the bioelectronic device to the D-phenylalanine (D-Phe) and L-phenylalanine (L-Phe) enantiomers. Reproduced with permission[68] Copyright 2019, Elsevier.

Figure 6: (a) Simplified electronic circuit to model an EGOFET bioelectronic sensor integrating a bio-recognition layer attached to the gate. **(b)** Calculated electric potential along the electrolyte domain in the case I) $C_G >> C_{OSC}$, II) $C_G \sim C_{OSC}$, and III) $C_G << C_{OSC}$. The corresponding ion and the hole charge distributions are displayed in **panel (c)**, **(d)** and **(e)**.

Figure 7: (a) EGOFET sensing transfer-characteristics, I_D *vs.* V_G at V_D = - 0.4 V, measured in the forward and reverse mode. The biomarker is the Human-Immunoglobulin-M while the gate is biofunctionalized with 10^{12} cm^{-2} anti-Human-Immunoglobulin-M. The base-line, I_0,

(red-line) is measured on the bio-functionalized gate incubated in phosphate-buffer-saline solution. Afterwards, the same gate is exposed, in sequence, to the following standard-solutions of Immunoglobulin-M at concentrations of: 6 zM (black-curve), $(6 \pm 3)\cdot 10$ zM (blue-curve), $(6 \pm 1)\cdot 10^2$ zM (light-green-curve), $(6.7 \pm 0.1)\cdot 10^3$ zM (magenta-curve) and $(6.67 \pm 0.01)\cdot 10^6$ zM (dark-green-curve). **(b)** I_D fractional change ($\Delta I/I_0$) *vs.* V_G at V_D = - 0.4 V for Immunoglobulin-M molecules ranging from 0 to $6\cdot 10^4$. The data and the colour-code are the same as in panel (a). While the bio-functionalized interface is incubated into the solution to be analyzed, the EGOFET responses are measured in deionized water to minimize the Debye-screening-length and maximize the response. **(c)** Gate-leakage-current, I_G *vs.* V_G as a function of Immunoglobulin-M detected concentrations. The concentrations are all marked with the same colour-code as in panel (a). Panel (a) – (c) Reproduced with permission[38] Copyright 2019, American Chemical Society. **(d)** Schematic of the self-assembled-monolayer (SAM) of recognition-elements, comprising both a mixed chemical SAM (chem-SAM) based on 3-mercaptopropionic acid (3-MPA) and 11-mercaptoundecanoic acid (11-MUA) in 10:1 ratio and a biological SAM (bio-SAM) of conjugated specific-capturing-antibodies. In the chem-SAM the hydrogen bonds are highlighted as red-arrows. θ defines the angle between a 3-MPA chain and the normal to the gate surface. **(e)** Direction and the occupancy (%) of the H-bonds resulting from the analysis of molecular dynamic trajectories under the gating-field. The color-codes indicate the percentage of frames in which the H-bond is established. In panel **(f)** the simulation is carried out on the same system as in panel (c) in which a defect, mimicking the affinity binding event, is simulated. Panel (d) – (f) Reproduced with permission[36] Copyright 2018, Springer Nature.

Figure 8: (a) Sketch of an OECT gallic acid sensor. Drain (D), source (S) and gate (G) electrode, are shown along with the PEDOT-PSS and the poly(diallyldimethylammonium chloride) (PDDA) and the multi-wall carbon nanotubes (MWNT) nanocomposite. The

oxidation of gallic acid at the PDDA-MWNT functionalized gate electrode is also shown on the right. **(b)** The potential drop profile occurring between the OECT gate and channel before (solid line) and after (dashed line) addition of gallic acid to the gating PBS solution. **(c)** Normalized current response to the increasing gallic acid concentration in PBS solution measured at V_D= 0.05 V and V_G= 0.6 V. Inset: current response at the detection limit ($\Delta I_S/\Delta I_N$ >3) of the device (10 nM), where ΔI_N is the channel current noise, ΔI_S the channel current response to 10 nM gallic acid; Panel (a) to panel (c) Reproduced with permission[85] Copyright 2017, Elsevier. **(d)** OECT bioelectronic sensor structure and a scheme of the biofunctionalization of PEDOT-PSS surface. **(e)** Cyclic voltammogram of the gate electrode in PBS i) before the gate functionalization, ii) after gate functionalization with the glucose oxidase complex and iii) in the presence of 10 mM of glucose. **(f)** Sensing mechanism. **(g)** Normalized calibration curves derived from the chronoamperometric response of the OECTs after successive additions of increasing concentrations of glucose. Inset shows the corresponding linear parts of the calibration curves. Panel (d) to panel (i) Reproduced with permission[79] Copyright 2016, John Wiley and Sons.

Figure 9: (a) Electrochemical potentials alignment of an Au or PEDOT-PSS electrode and the $Fe(CN)_6^{4-}$ / $Fe(CN)_6^{3-}$ redox couple and the Fe^{II} oxidation to Fe^{III} is also illustrated. **(b)** An electrochemical cell where the oxidation of a Fe^{II} to Fe^{III} is featured against an Ag/AgCl (KCl sat.) reference electrode producing a Faradaic-current. **(c)** Cyclic voltammetry of: Au in KCl 0.1 M (black solid line) and in 1 mM $K_4[Fe(CN)_6] \cdot 3H_2O$ in 0.1M KCl (red solid line); Au / PEDOT-PSS in KCl 0.1 M (black dotted line) and in 1 mM $K_4[Fe(CN)_6] \cdot 3H_2O$ in 0.1M KCl (red dotted line). Scan rate 0.1 Vs^{-1}.

Figure 10: (**a**) Cyclic voltammetry results of $K_3Fe(CN)_6/K_4Fe(CN)_6$ in KCl solution for different thicknesses of PEDOT-PSS (5%) DMSO electrodes Reproduced with permission.[60]

Copyright 2018, National Academy of Sciences. **(b)** Schematic diagram of charge transport (red dotted lines) within the polymer electrode and the electron transfer (black arrows) at the polymer electrolyte interface. The blue lines are pictorial view of the PEDOT chains aggregates that hold short-range order through π–π stacks. **(c)** Illustration of the amperometric transduction of an electrochemical reaction with an OECT.

Rosaria Anna Picca is researcher in Analytical Chemistry at the Chemistry Department of the University of Bari. She received the PhD in "Chemistry and physics for the environment" in 2008. Her research activities deal with the application of electrochemical and surface analytical techniques in the field of material science, in particular for the preparation and characterization of nanostructured materials. She is also involved in the development and study of organic field-effect transistor biosensors. She is co-author of more than 50 publications and 4 book chapters.

Kyriaki Manoli received her B.Sc. in Chemistry in 2003 from the University of Ioannina, Greece and her M.Sc. and PhD in "Polymer Science and its Applications" from the Chemistry Department of the National and Kapodistrian University of Athens - Greece in 2005 and 2010 respectively. In 2011 she joined the Analytical Chemistry Department at the University of Bari as a post-doctoral fellow. From 2016 she is a researcher at the same department. Her research interests include fabrication and characterization of functional electronic devices that embed biological elements and, in particular, field- effect transistors to be used for chemical and bio- sensing applications.

Luisa Torsi is professor of chemistry and she received her *laurea* degree in Physics and the PhD in Chemical Sciences from the University of Bari and was post-doctoral fellow at Bell Labs. She was awarded with the H.E. Merck prize, with the 2019 Distinguished Women Award by the International Union of Pure and Applied Chemistry and the 2019 Robert Kellner Lecturer by the European Chemical Society Division of Analytical Chemistry. Her research interests span from analytical biosensors, to organic electronic devices and electrochemistry; but also, electronic and interfacial properties of conducting and semiconducting polymers and nanomaterials.

Organic bioelectronic sensors are promising for point-of-care health monitoring. The rational design of highly performing potentiometric sensors is proposed to fully exploit the high potential of electrolyte-gated field-effect transistors. Amperometric electrochemical transistors for metabolites assay are reviewed too. A critical perspective on both configurations is offered, to improve materials and devices structures enabling ultimate sensitivity, selectivity and fast response.

Keyword: Organic Bioelectronic Sensor

Rosaria Anna Picca, Kyriaki Manoli, Eleonora Macchia, Lucia Sarcina, Cinzia Di Franco, Nicola Cioffi, Davide Blasi, Ronald Österbacka, Fabrizio Torricelli, Gaetano Scamarcio and Luisa Torsi*

Ultimately sensitive bioelectronic sensor by materials and device structures design

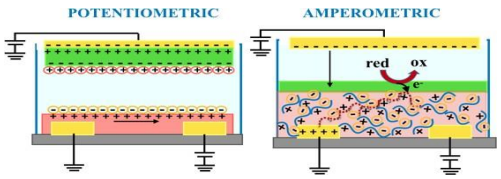

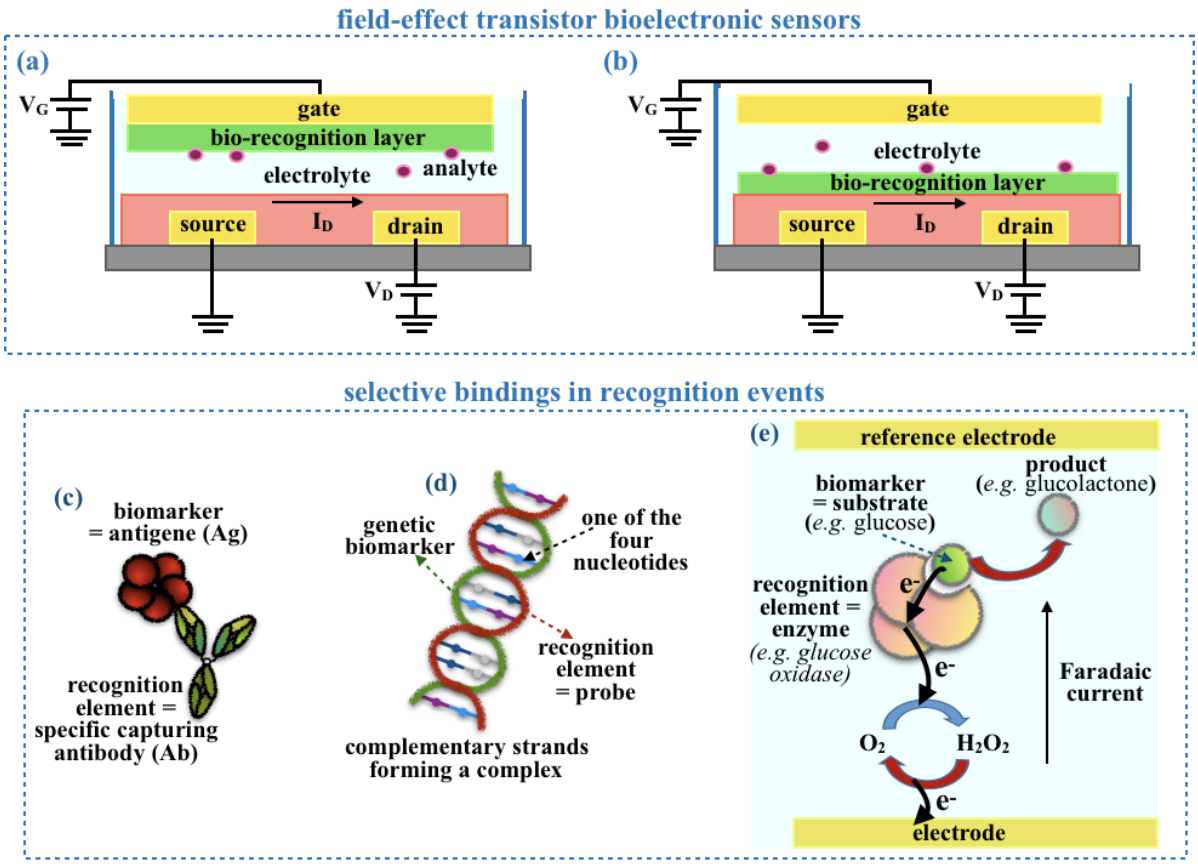
field-effect transistor bioelectronic sensors
(a)
V_G
gate
bio-recognition layer
electrolyte
analyte
source
I_D
drain
V_D
(b)
V_G
gate
electrolyte
bio-recognition layer
source
I_D
drain
V_D
selective bindings in recognition events
(c)
biomarker
= antigene (Ag)
recognition
element =
specific capturing
antibody (Ab)
(d)
genetic
biomarker
one of the
four
nucleotides
recognition
element
= probe
complementary strands
forming a complex
(e)
reference electrode
biomarker
= substrate
(e.g. glucose)
product
(e.g. glucolactone)
recognition
element =
enzyme
(e.g. glucose
oxidase)
e-
e-
Faradaic
current
O_2
H_2O_2
e-
electrode

Figure 1


materials and operational details
ion impermeable OSC
(a)
P3HT
PBTTT-14
P3HT
electrolyte-gated OFET
(c)
gate
VG
CG
bio-recognition layer
CBIO
IG << ID
COSC
2D / 3D
source
ID
drain
VD
ion permeable organic semiconductors
(b)
PSS -
PSS- =
PEDOT +
PEDOT + =
PSS -
PEDOT +
nanofibrils
PEDOT + PSS -
organic electrochemical transistor
(d)
gate
VG
IG
red
ox
e-
drain
source
VD

Figure 2

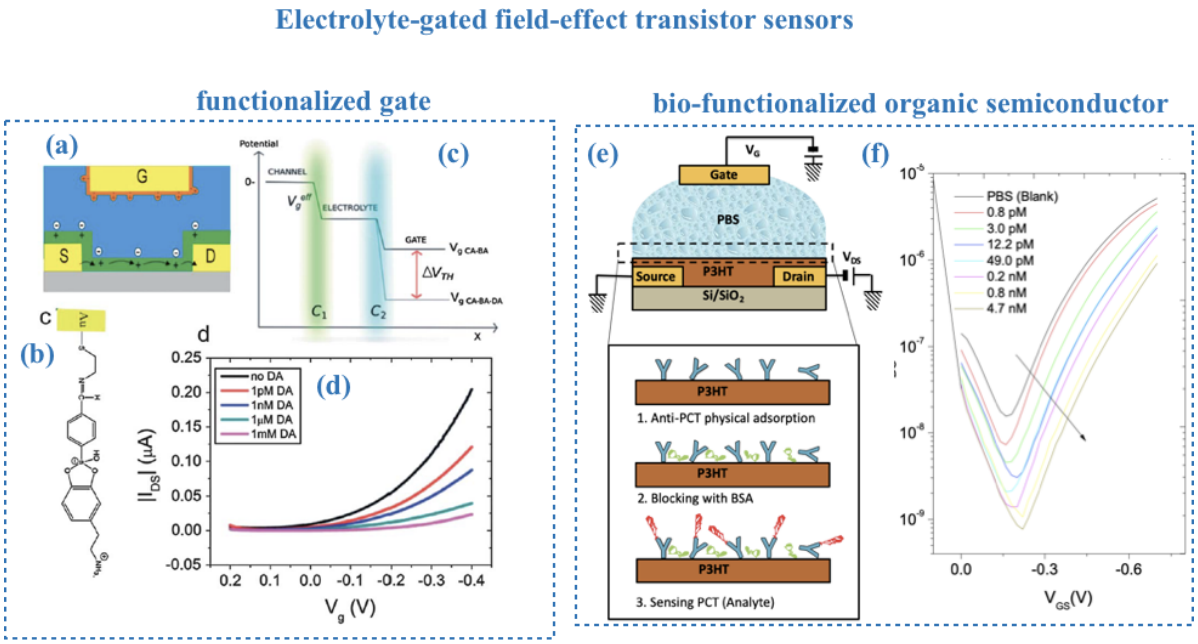
Electrolyte-gated field-effect transistor sensors
functionalized gate
bio-functionalized organic semiconductor
(a)
G
S
D
(b)
(c)
Potential
CHANNEL
ELECTROLYTE
GATE
x
(d)
no DA
1pM DA
1nM DA
1μM DA
1mM DA
$|I_{DS}|$ (μA)
V_g (V)
(e)
Gate
PBS
Source
P3HT
Drain
Si/SiO2
1. Anti-PCT physical adsorption
2. Blocking with BSA
3. Sensing PCT (Analyte)
(f)
PBS (Blank)
0.8 pM
3.0 pM
12.2 pM
49.0 pM
0.2 nM
0.8 nM
4.7 nM
V_{GS}(V)

Figure 3

label-free single molecule detection with large *electrolyte-gated FETs*
bio-functionalization of the gate electrode

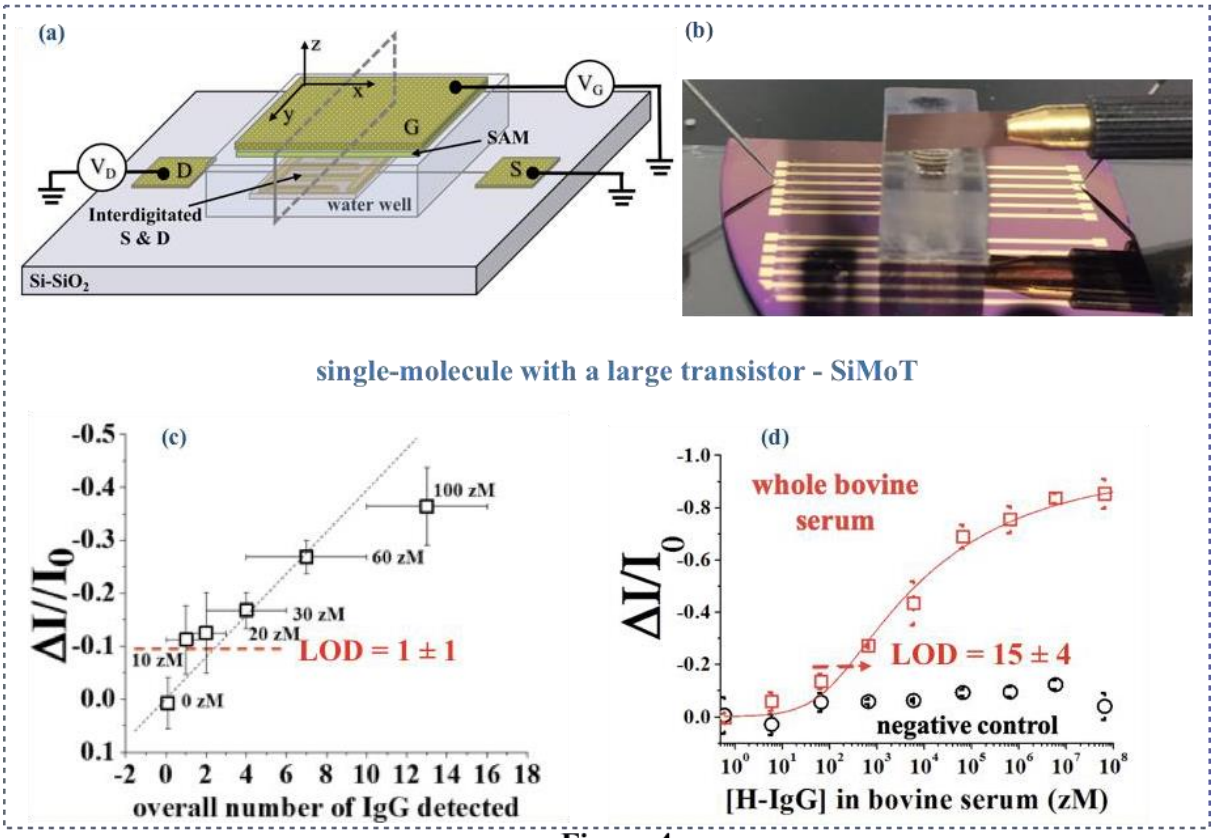

Figure 4

label-free single molecule detection with large *electrolyte-gated FETs*

bio-functionalization of theFET channel

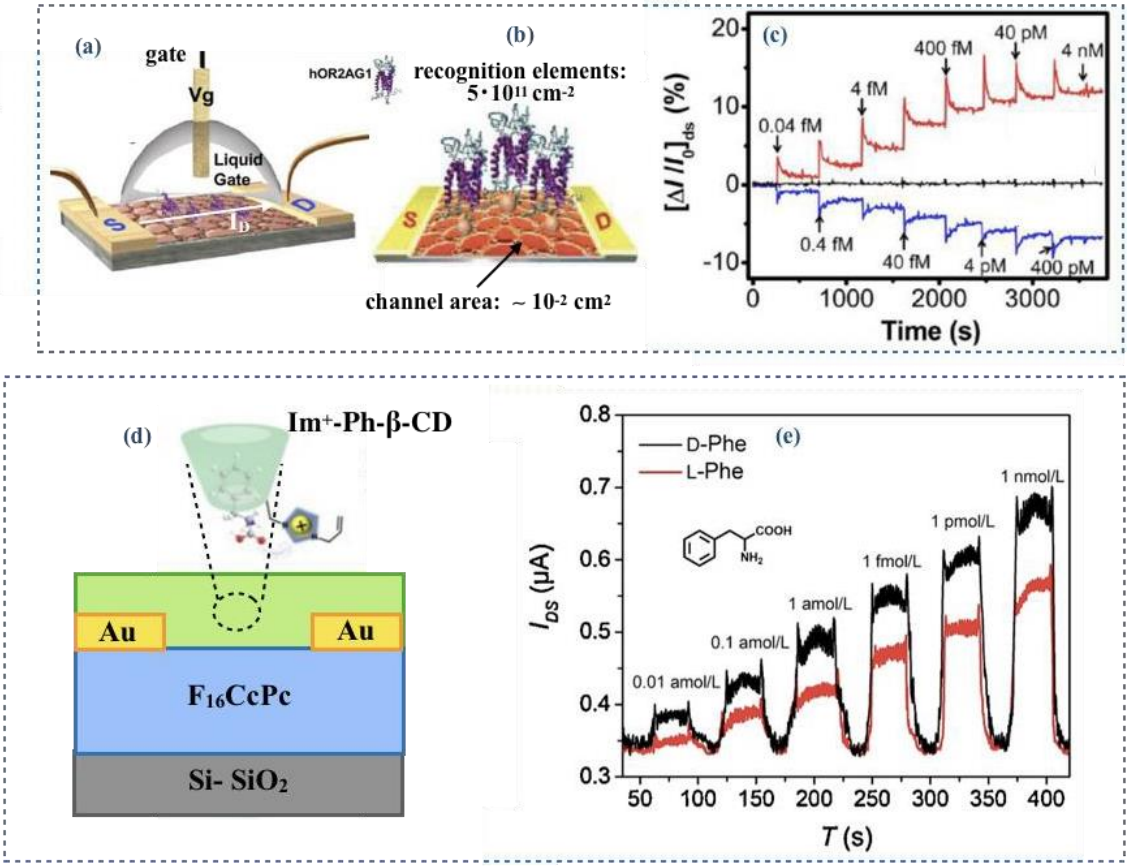

Figure 5

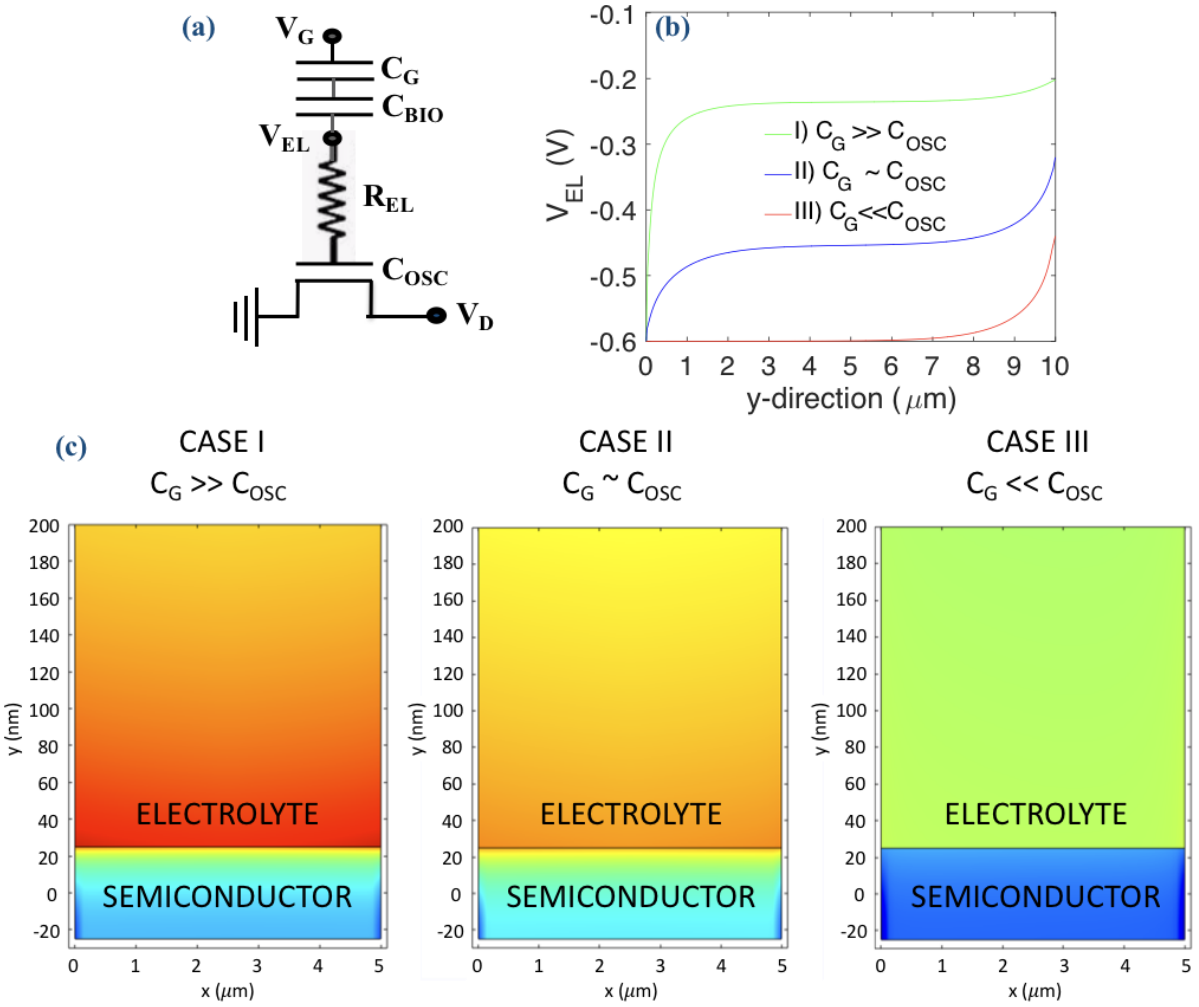
(a)
V_G
C_G
C_{BIO}
V_{EL}
R_{EL}
C_{OSC}
V_D
(b)
V_{EL} (V)
y-direction (μm)
I) C_G >> C_{OSC}
II) C_G ~ C_{OSC}
III) C_G<<C_{OSC}
(c)
CASE I
C_G >> C_{OSC}
CASE II
C_G ~ C_{OSC}
CASE III
C_G << C_{OSC}
ELECTROLYTE
SEMICONDUCTOR
y (nm)
x (μm)

Figure 6

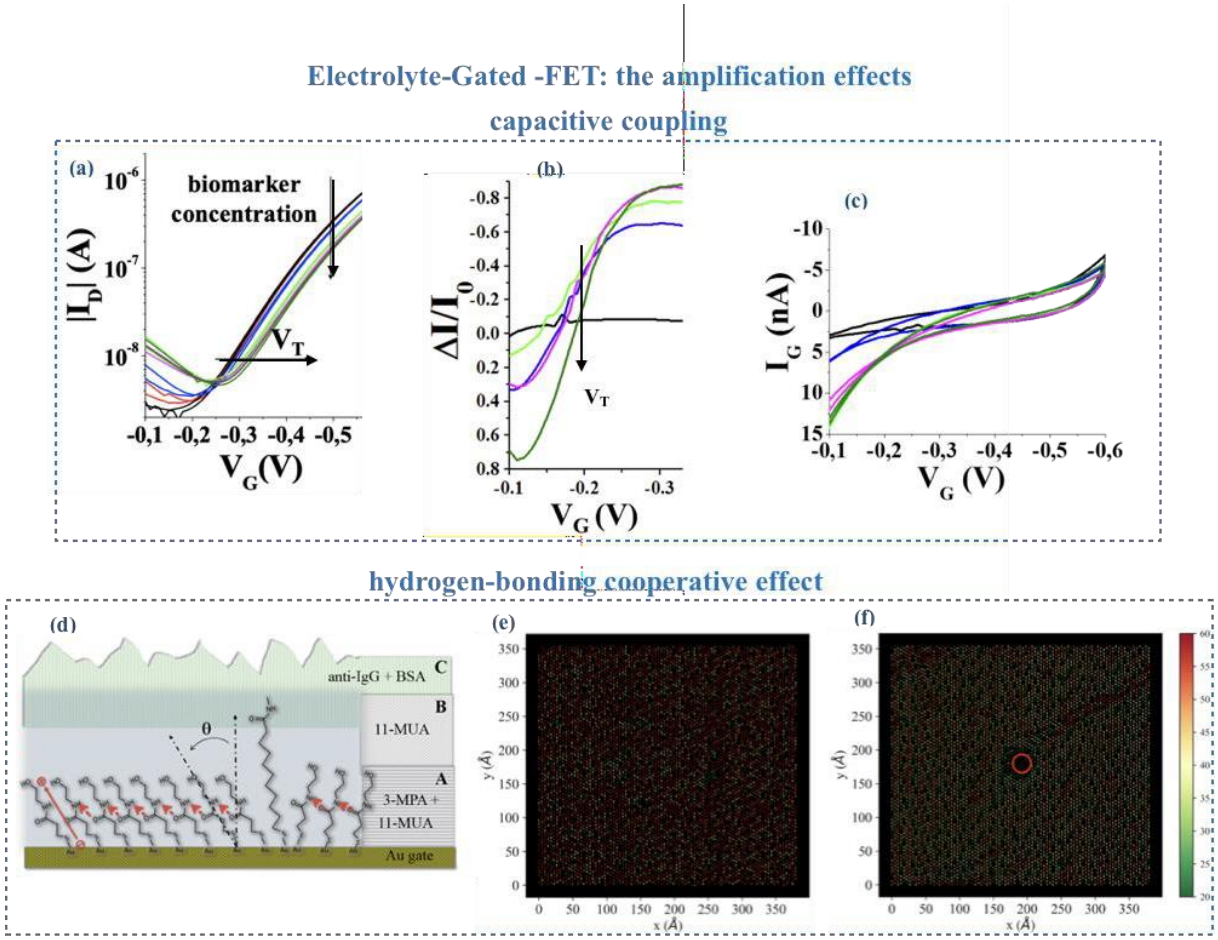
Electrolyte-Gated -FET: the amplification effects
capacitive coupling
(a)
biomarker concentration
$|I_D|$ (A)
V_T
V_G(V)
(b)
$\Delta I/I_0$
V_T
V_G (V)
(c)
I_G (nA)
V_G (V)
hydrogen-bonding cooperative effect
(d)
anti-IgG + BSA
C
B
11-MUA
θ
A
3-MPA + 11-MUA
Au gate
(e)
y (Å)
x (Å)
(f)
y (Å)
x (Å)

Figure 7

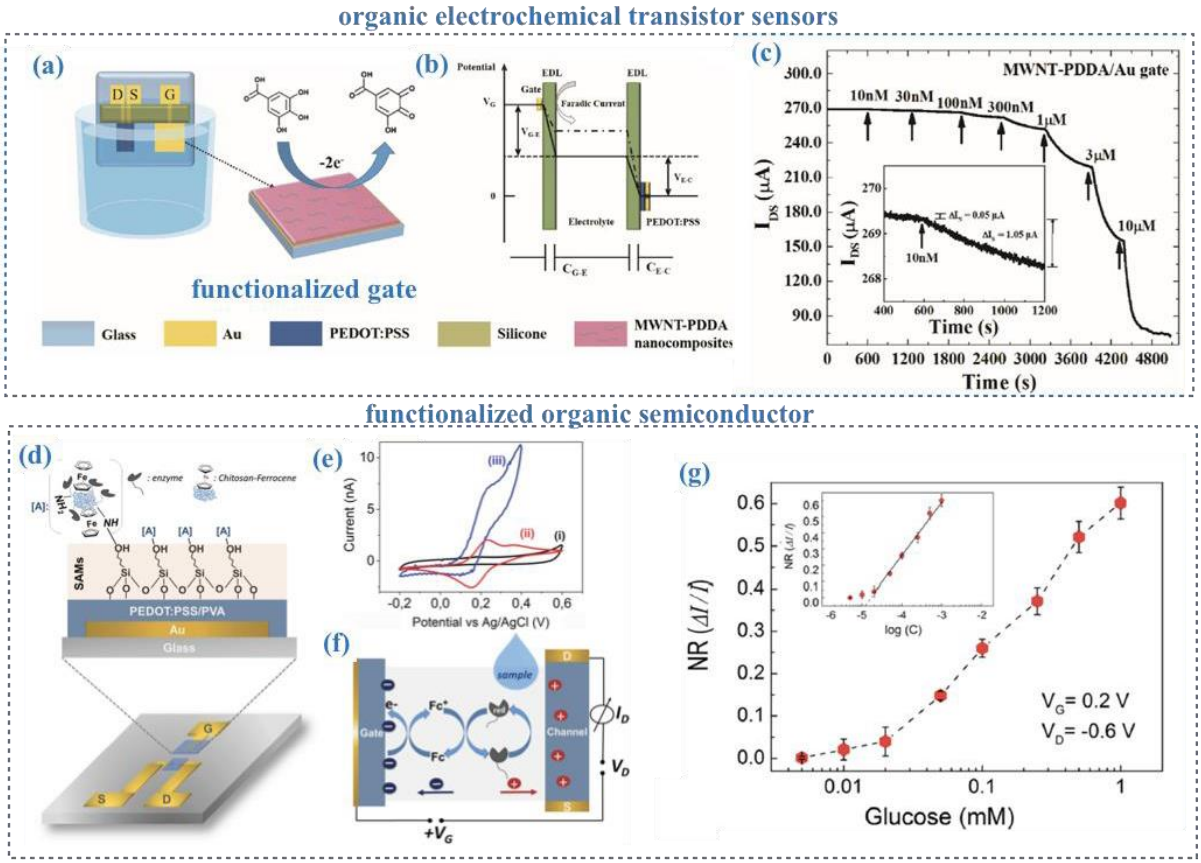
organic electrochemical transistor sensors
(a)
D S G
-2e⁻
functionalized gate
Glass
Au
PEDOT:PSS
Silicone
MWNT-PDDA nanocomposites
(b)
Potential
EDL
EDL
Gate
Faradic Current
Electrolyte
PEDOT:PSS
(c)
MWNT-PDDA/Au gate
10nM 30nM 100nM 300nM 1μM 3μM 10μM
Time (s)
functionalized organic semiconductor
(d)
: enzyme
: Chitosan-Ferrocene
SAMs
PEDOT:PSS/PVA
Au
Glass
(e)
Current (nA)
Potential vs Ag/AgCl (V)
(f)
sample
Gate
Channel
(g)
NR (ΔI/I)
log (C)
V_G = 0.2 V
V_D = -0.6 V
Glucose (mM)

Figure 8

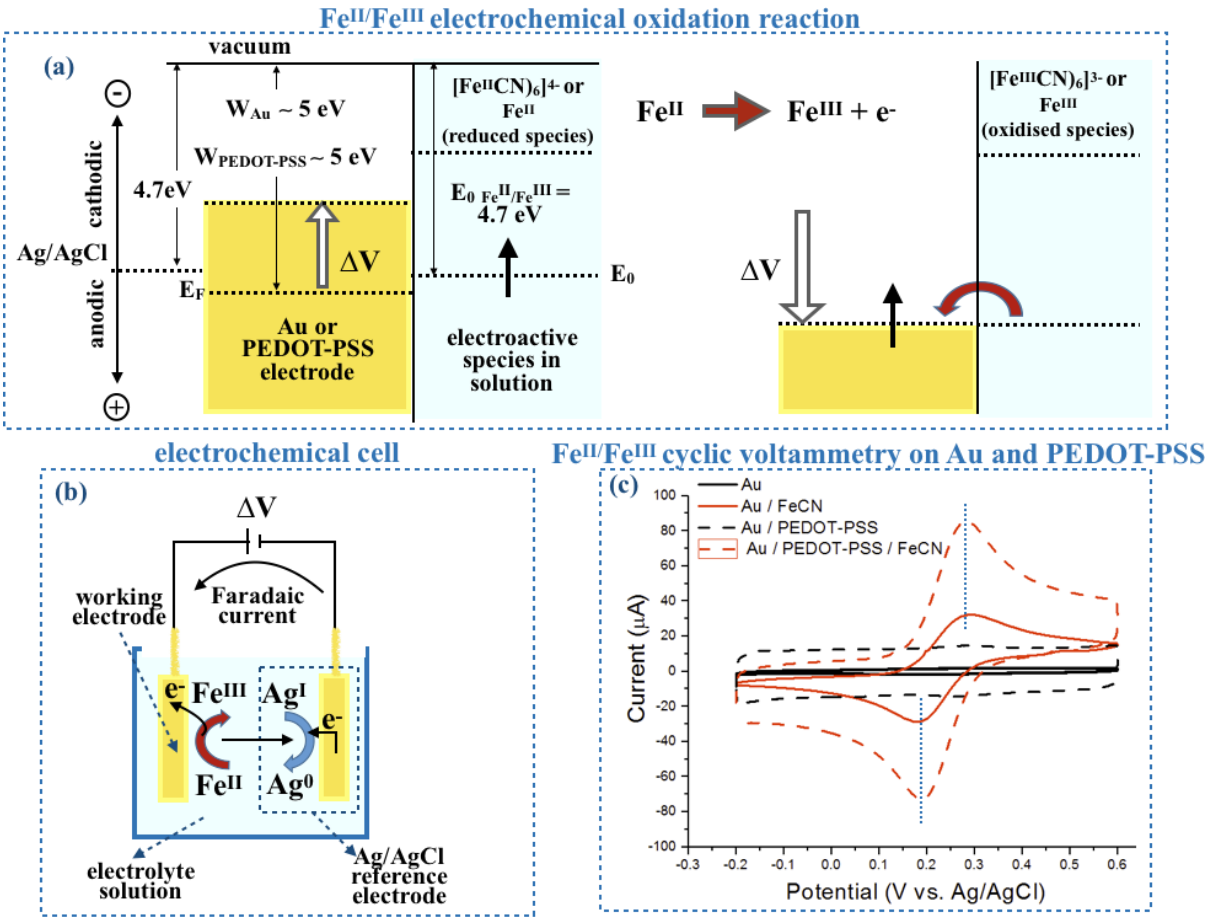
FeII/FeIII electrochemical oxidation reaction
(a)
vacuum
WAu ~ 5 eV
WPEDOT-PSS ~ 5 eV
4.7eV
cathodic
Ag/AgCl
anodic
EF
ΔV
Au or PEDOT-PSS electrode
[FeIICN)6]4- or FeII (reduced species)
E0 FeII/FeIII = 4.7 eV
E0
electroactive species in solution
FeII → FeIII + e-
[FeIIICN)6]3- or FeIII (oxidised species)
ΔV
electrochemical cell
(b)
ΔV
working electrode
Faradaic current
e-
FeIII
AgI
e-
FeII
Ag0
electrolyte solution
Ag/AgCl reference electrode
FeII/FeIII cyclic voltammetry on Au and PEDOT-PSS
(c)
Au
Au / FeCN
Au / PEDOT-PSS
Au / PEDOT-PSS / FeCN
Current (μA)
Potential (V vs. Ag/AgCl)

Figure 9

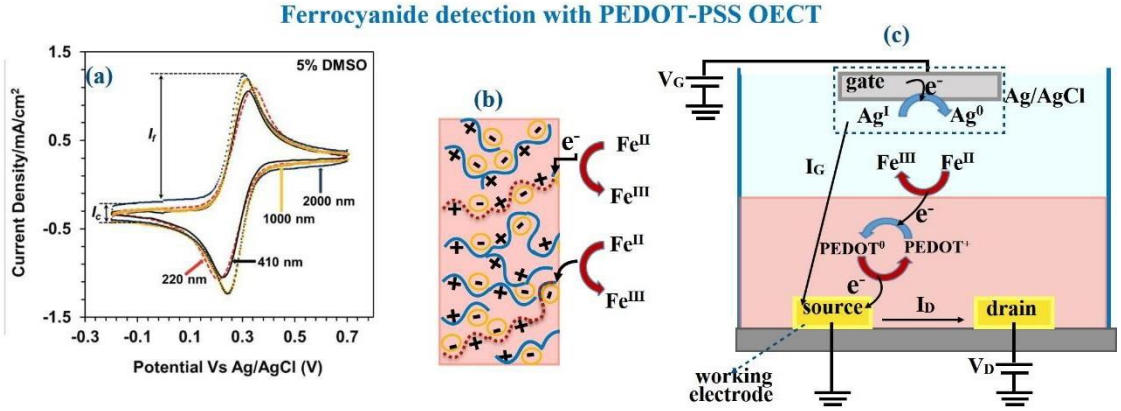
Ferrocyanide detection with PEDOT-PSS OECT
(a)
5% DMSO
Current Density/mA/cm²
Potential Vs Ag/AgCl (V)
2000 nm
1000 nm
410 nm
220 nm
(b)
(c)
gate
Ag/AgCl
source
drain
working electrode

Figure 10